A MASTER′S THESIS

A STUDY ON THE NEARSHORE CURRENT USING NONLINEAR PARABOLIC MILD SLOPE AND QUASI-3D EQUATION

JEJU NATIONAL UNIVERSITY GRADUATE SCHOOL

Department of Civil & Ocean Engineering

Seung-Hyun An

February 2010

A STUDY ON THE NEARSHORE CURRENT USING NONLINEAR PARABOLIC MILD SLOPE AND QUASI-3D EQUATION

Seung-Hyun An

(Supervised by Professor Nam-Hyeong Kim)

A thesis submitted in partial fulfillment of the requirement for the degree of

Master of Engineering

2010. 2

Department of Civil & Ocean Engineering

GRADUATE SCHOOL

JEJU NATIONAL UNIVERSITY

CONTENTS

List of Figures

List of Tables

Summary

The nearshore regions are very important places where are closely related with human civilization. In particular, Korea, the peninsula country, is close to the ocean so the nearshore regions have been used as distribution facilities such as harbors connecting rand and ocean transportation. Recently, due to the increase in the peoples' leisure time, the importance of nearshore regions adjacent to recreation areas and tourist attractions has been increasing. Thus, preservations and maintenances of nearshore regions have been issued.

In nearshore regions, the causes of sediment transport and shoreline erosion are waves, nearshore currents, the tide, wind, and the outflow of rivers. The most important cause among these has known as nearshore current.

When the water circulation system is changed by constructing artificial construction at the nearshore region, the balance in the sediment system will then be broken. Consequently, the shoreline and cross-profile may be damaged seriously. In fact, many problems such as erosion and accumulation by sediment transport occurred. Therefore, studies on the nearshore current are necessary to effectively use the nearshore area.

In this study, by using nonlinear parabolic mild slope and Quasi-3d equations, the circulation phenomena are simulated. When the numerical analysis is carried out, the numerical result of the wave model is calculated by the circulation model after input wave data are computed by the wave model. Through the above simultaneous process, the water circulation phenomena are analyzed, for the nearshore current is generated by wave-current interaction.

The numerical models used in this study are compared with observational result and numerical result of previous literature so proprieties of the numerical models are verified. The verification models are circulation phenomenon of the nearshore current in the coast established detached breakwater and inclined coast, and good agreements are obtained.

Circulation tendencies of the nearshore current using the numerical model in this study are computed. Study areas are Gangjeong Waters, Jeju and Haeundae Waters, Busan, respectively. The numerical analysises at Gangjeong, Jeju are performed to examine variations of the nearshore current caused by constructing artificial constructions, and those at Haeundae, Busan are performed to see effects of the wind stresses.

As a result, the understanding of the water circulation system within nearshore area is improved, and it is therefore considered that it can be applied to developing and utilizing the nearshore regions effectively.

CHAPTER 1
INTRODUCTON

1.1 Background

Within the ocean, there are a variety of types of flows, such as an ocean current flowing nearly uniformly, a tidal current caused by a tide, and a nearshore current generated by the interaction between waves and currents in the vicinity of the surfzone. Of these, the nearshore current is a very important phenomenon for the shoreline deformation due to alongshore sediment transport, bottom-topography deformation caused by cross-shore sediment transport and the diffusion of pollutant within the nearshore regions.

While the existence of a nearshore current within onshore zone has been recognized experientially, it is relatively recently that nearshore currents have became the subject of scientific study. Since the nearshore system, or the nearshore circulation pattern, was proposed by Shepard-Inman (1950), both domestic and international studies on the nearshore current have progressed. In particular, since the development of the model for a nearshore current including radiation stress by Longuet-Higgins and Stewart (1964), studies on nearshore currents have rapidly advanced. Sonu (1972) executed a large-scale site survey and attempted to estimate nearshore currents quantitatively.

In addition, many studies and applications of nearshore currents have been carried out by a considerable number of experts and researchers, such as Berkhoff(1972), Noda et al.(1974), Sasaki(1975), Liu and Mei(1976), Birkemeir and Dalrymple(1980), Kirby and Dalrymple(1983, 1986), Nishimura(1987), Min et al.(1993), Kim and Lee(1998), Putrevu and Svendsen (1999), Ham et al. (2002), and Shi, Kirby and Hanes (2007).

However, results from domestic studies on the nearshore current are less sufficient than those obtained from abroad. Over the past several decades in Korea, studies concentrating on

the development of the onshore zone have been carried out preferentially because domestic situations have focused on the growth of the economy. Consequently, various problems have occurred related to coastal engineering such as erosion and deposition of the coast. Thus, studies on the nearshore current have been actively progressing in order to understand the feature of water flows and unveil ultimately causes of problems of coastal engineering.

1.2 Objectives

The water flow phenomena in onshore zone are various types of the ocean current, the tidal current, the drift current, the wave-induced current, and so forth. Causes of generations differ in each flow phenomenon. Most of previous studies on the water flow phenomena research mainly these flows independently. However, the flow phenomena within surfzone are made by more complex mechanism. They are generated by wave-current interactions and named as the "Nearshore Current". The nearshore currents consist of the longshore currents and rip currents, and longshore currents and rip currents affect the longshore and cross-shore sediment transport considerably.

Such longshore and cross-shore sediment transports are closely related with human's civilization and the ocean ecosystem, and to do this, it is necessary to perform a study on the nearshore current.

In this study, it is objective to develop the numerical model that can describe flow phenomena of the nearshore currents generated by wave-current interaction. In order to simulate variations of the nearshore current exactly, deformations and interactions between waves and currents should be considered. To do this, the numerical model used in this study couples wave module with circulation module.

Through such study, a quantitative analysis about the nearshore current is possible, and understanding for the water circulation system within onshore zone can be improved. Therefore, it is considered that positive solutions about coastal engineering problems such as changes of topographic and deformations of coast can be gained.

1.3 Study Contents

As described above paragraph, the nearshore current is generated by the wave-current interaction. Thus, wave and circulation analysises are simultaneously carried out. And in this study, the nonlinear parabolic mild slope equation by which diffractions, refractions, and breakings of the wave can be computed is used for calculating the deformation of propagating wave, and Quasi-3D equation by which the variations of velocity profile according to water depth can be considered is used for calculating circulation phenomena of flows.

In this study, flux boundary condition is added to the numerical model by volume flux method in order to perform more exact numerical analysis, and the ADI method, one of implicit method, is used to perform effective numerical analysis.

To verify the numerical model used in this study, results of it is compared with those obtained from the observation by Watanabe and Maruyama (1984) and the numerical analysis using Boussinesq equation by Nishimura (1984).

As the applications of the numerical model, a behavior of the nearshore current caused by establishing artificial coastal constructions that may influence the flow within nearshore current is simulated so it is examined whether effects of artificial constructions are corresponded with the purpose of their installation or not. It is also examined how the wind-induced surface shear stress influences the flow behaviors. Study sites are Gangjeong Waters, Jeju and Haeundae Waters, Busan.

CHAPTER 2
Basic Equation for Wave Model

2.1 Mild Slope Equation

Berkhoff (1972) noted that problems of linear progressive waves could be predicted by a weighted vertically integration method. The vertical integration method reduces the problems to simply the two horizontal dimensions, x and y. The equation of Berkhoff is known as the Mild Slope Equation (MSE). It is written as follows:

$$\nabla_h \cdot (CC_g \nabla_h \phi) + \sigma^2 \frac{C_g}{C} \phi = 0 \tag{1}$$

where C and C_g are the wave velocity and group velocity, respectively. Also, ϕ is a velocity potential depending on the time.

$$C = \sqrt{(g / k) \tanh kh} \tag{2}$$

$$C_g = C / 2(1 + 2kh / \sinh 2kh) \tag{3}$$

where h, g, σ and k are the water depth, the acceleration of gravity, the relative angular frequency of the waves, and the wave number, respectively. Also, these are expressed as the following dispersion relationship equation:

$$\sigma^2 = gk \tanh kh \tag{4}$$

The above dispersion relationship equation is again derived to consider the Doppler Effect. It is as follows and shown in Fig. 1.

$$C_a = C_r + U \cos \alpha \tag{5}$$

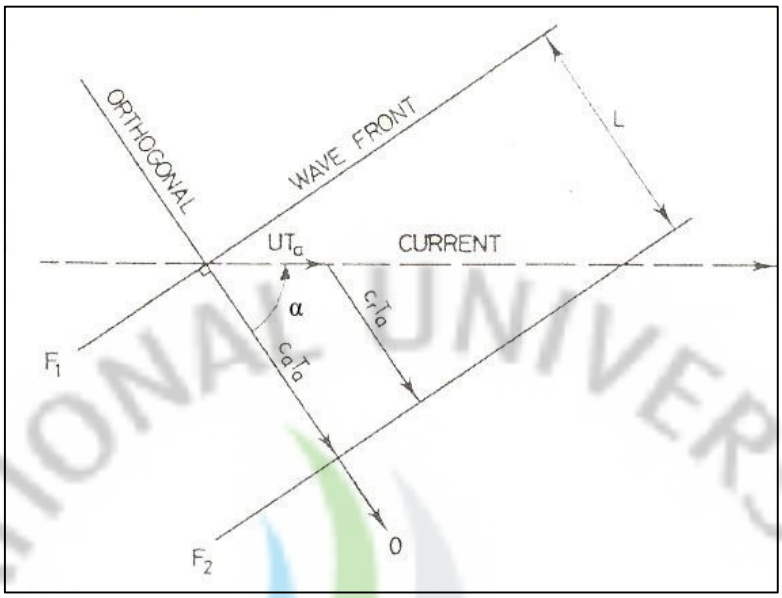

Fig. 1 Relation between absolute and relative phase velocity for wave in steady uniform current (form Jonsson, 1989)

where $C_a = \sigma_a / k_a$ is the absolute phase velocity, and $C_r = \sigma_r / k_r$ is the relative phase velocity. When the effect of the current on the wave is reflected, then $k_a = k_r$ because the wave length can appear to be the same. Hence, the dispersion relationship equation, Eq. (2), is again derived to reflect the Doppler Effect and the rectified equation is as follows:

$$\sigma_a = \sigma_r + kU \cos\alpha \tag{6}$$

In the wave with current, the wave orthogonals and the wave rays generally have different directions. The wave orthogonals are defined as perpendicular to the wave front. A wave ray, on the other hand, is defined as the direction along which the wave energy is moving. Thus, $C_{ga} = C_{gr}$, and by assuming that the wave is primarily propagating in the x direction, Eq. (4) can be rewritten as follows:

$$\sigma_a = \sigma_r + kU \tag{7}$$

Consequently, the new form of Eq. (2) is as follows:

$$(\sigma_a - kU)^2 = gk \tanh kh \tag{8}$$

Eq. (8) is employed all over the domain of calculation of the numerical model used in this study.

2.2 Parabolic Equation

Since the linear mild slope model was proposed by Berkhoff (1972), numerous researchers have improved the model. Radder (1972) developed a parabolic mild slope model as follows:

$$2ikCC_g A_x + 2k(k - k_0)CC_g A + i(kCC_g)_x A + (CC_g A_y)_y = 0 \tag{9}$$

Radder's equation had several advantages over the elliptic form proposed by Berkhoff (1972). First, the boundary problems inside the domain of the model are simplified. Second, a very effective numerical analysis is available for the finite difference form. Radder also separated the wave into forward and backward propagating components by using the splitting matrix approach to the linear mild slope elliptic model of Berkhoff (1972). However, the model of Radder (1979) has a restriction which the waves should propagate within 45° of the assumed wave direction. Thereafter, Booij (1981) also improved on the elliptic mild slope equation using the Helmholtz equation, and his equation included more terms of approximation than the previous equation. It also has the ability to handle waves propagating within 60° of the assumed wave direction.

More recently, Kirby (1986) have developed an extension form of Booij's approximation using the Minimax method, which is able to deal with wider propagation waves for diffraction and refraction.

2.3 Diffraction Model for Parabolic Equation

Because the mild slope equation assumes that a water depth is linearly decreased, applications for real bathymetry are restricted. Mei and Tuck (1980) developed a simple parabolic equation for wave diffraction and applied it for the diffraction of waves by an island. Their equation is as follows:

$$2ikA_x + A_{yy} = 0 \tag{10}$$

where A is the complex amplitude related to the water surface displacement η.

$$\eta = Ae^{i(kx-\sigma t)} \tag{11}$$

Eq. (10) is obtained simply by the condition of $k - k_0 = 0$ for constant depth in Eq. (9). Yue and Mei (1980), using the multiple scale method, developed a nonlinear form of Eq. (10), which can effectively describe the diffraction of the wave.

2.4 Nonlinear Combined Refraction and Diffraction Model

Kirby and Dalrymple (1983) improved the original mild slope equation by considering nonlinear effects. Because the mild slope equation is inherently linear, Kirby and Dalrymple (1983) used a Lagrangian approach and a multiple scale technique to consider nonlinear effects. Their equation is as follows:

$$2ikCC_g A_x + 2k(k - \overline{K})CC_g A + i(kCC_g)_x A + (CC_g A_y)_y - kCC_g K' |A|^2 A = 0 \tag{12}$$

where K' is defined as:

$$K' = k^3 \frac{C}{C_g} D \tag{13}$$

Here, D is as follows:

$$D = \frac{\cosh 4kh + 8 - 2\tanh^2 kh}{8\sinh^4 kh} \tag{14}$$

In Eq. (12), the nonlinearity is only represented by the last term composed of Eqs. (13) and (14).

2.5 Wave-current Interaction Model

Booij (1981), using a Lagrangian approach, proposed the corrected form of the mild slope equation including the influence of current. Kirby and Dalrymple (1983) also developed an equation of an expanded form of Booij's equation. This equation includes a nonlinear correction and the ability to handle a stronger current than Booij's equation. The equation of Kirby and Dalrymple (1983) is as follows:

$$\begin{aligned}&(C_g + U)A_x + VA_y + i(\bar{k} - k)(C_g + U)A \\ &+ \frac{\sigma}{2}\left[\frac{C_g + U}{\sigma}\left(\frac{\partial}{\partial x}\right) + \left(\frac{\partial}{\partial y}\right)\right]\left[\frac{C_g + U}{\sigma}A - \frac{i}{2\sigma}\left(\left(p - V^2\right)A_y\right)\right]_y \\ &- \sigma\frac{k^2}{2}D|A|^2 A = 0\end{aligned} \tag{15}$$

where $p = CC_g$, and $\bar{k}$ is taken as the average wave number along the y-axis. U and V are the velocities of the x-direction and the y-direction, respectively. The nonlinear term D is given by Eq. (14).

Kirby (1986) developed an expanded form of Eq. (15) to handle waves having a wide incident angle. This equation includes the more accurate minimax approximation and is given by:

$$
\begin{aligned}
&(C_g+U)A_x - 2\mathrm{D}_1 V A_y + i(\bar{k}-a_0 k)(C_g+U)A \\
&+\left(\frac{C_g+U}{2\sigma}\right)\left(-\mathrm{D}_1\sigma\frac{\partial A}{\partial y}\right)_x + i\mathrm{D}\left(p-V^2\right)\frac{\partial A}{\partial y} \\
&-i\mathrm{D}_1 UV\frac{\partial A}{\partial y} + UV\frac{\partial A}{\partial x} + \frac{i\sigma k^2}{2}D|A|^2 A \\
&+\left(\frac{\omega}{2}+\frac{-b_1}{k}\right)\left(p-V^2\right)\frac{\partial A}{\partial y} + 2i\sigma V\frac{\partial A}{\partial x} \\
&+b_1\beta\left[2i\omega U\frac{\partial A}{\partial x} + 2i\sigma V\frac{\partial A}{\partial y} - 2UV\frac{\partial A}{\partial xy} + \left(p-V^2\right)\frac{\partial A}{\partial y}\right] \\
&-\frac{i}{k}b_1\left\{(\omega V)_y + 3(\omega U)_x\right\}\frac{\partial A}{\partial x} - \mathrm{D}_2 b_0 U\frac{\partial A}{\partial x} + \frac{1}{2}\omega U_x\frac{\partial A}{\partial x} \\
&+ik\omega U(a_0-1)\frac{\partial A}{\partial x} = 0
\end{aligned}
\tag{16}
$$

where $\beta = \frac{k_x}{k^2} + \frac{\left(k\left(p-U^2\right)\right)_x}{2k^2\left(p-U^2\right)}$, $\Delta_1 = a_1 - b_1$, $\Delta_2 = 1 + 2a_1 - 2b_1$, and $\Delta\phi = a_1 - b_1\frac{\bar{k}}{k}$.

The coefficients a_0, a_1, and b_1 depend on the aperture width determined to specify the minimax approximation by Kirby (1986). These are used in this study as follows:

$$
\begin{aligned}
a_0 &= 1 \\
a_1 &= -0.75 \\
b_1 &= -0.25
\end{aligned}
\tag{17}
$$

In this study, in order to consider wave-current interactions, equation (16), as proposed by Kirby (1986), is used.

2.6 Wave Breaking Model

For wave breaking, Dally et al. (1985) showed that the rate of loss of wave energy fluxes is dependent on the excess of energy flux over a stable value. It has been tested for various bottom slopes and successfully predicts the wave height in the surfzone. This model is expressed by Kirby and Dalrymple (1986) as the wave breaking dissipation equation, which is given as:

$$\omega = \frac{KC_g(1-(\gamma h/H)^2)}{h} \tag{18}$$

where K and γ are empirical constants of 0.017 and 0.4, as determined by Dally et al. (1985). Also, wave height, $H = 2|A|$ and the breaking index relation ($H > 0.78h$) is used to determine the existence of wave breaking.

2.7 Radiation Stress

Generally, radiation stresses have been known as the most important factor of the nearshore current phenomenon. Thus, the determination of a radiation stress is very important. In this study, radiation stresses needed for the numerical analysis process are defined as:

$$S_{\alpha\beta} = \overline{\int_{-h_o}^{\zeta} (pu_{\omega\alpha}u_{\omega\beta} + p\delta_{\alpha\beta})dz} - \delta_{\alpha\beta}\frac{1}{2}\rho g h^2 \tag{19}$$

where $\delta_{\alpha\beta}$ is the Kronecker delta function. Also, $u_{\alpha\beta}$ is the horizontal short-wave-induced velocity and h is the mean water surface elevation. The generalized radiation stress tensor is also given as:

$$S_{\alpha\beta} = e_{\alpha\beta}S_m + \delta_{\alpha\beta}S_p \tag{20}$$

Where $e_{\alpha\beta}$ is defined as follows:

$$e_{\alpha\beta} = \begin{bmatrix} \cos^2\theta & \sin\theta\cos\theta \\ \sin\theta\cos\theta & \sin^2\theta \end{bmatrix} \tag{21}$$

Thus, Eq. (20) also can be written as in terms of (x, y) as follows:

$$S_{\alpha\beta} = \begin{Bmatrix} S_{xx} & S_{xy} \\ S_{yx} & S_{yy} \end{Bmatrix} \tag{22}$$

The scalars S_m and S_p are defined as:

$$S_m = \overline{\int_{-h_o}^{\zeta} \rho u^2{}_{\omega} dz} \tag{23}$$

$$S_p = -\overline{\int_{-h_o}^{\zeta} \rho \omega^2{}_{\omega} dz} + \frac{1}{2}\rho g \overline{\eta^2} \tag{24}$$

where surface displacement $\eta = \zeta - h$.

Outside the surfzone, Eqs. (23) and (24) can be written as the results for sinusoidal waves.

$$S_m = \frac{1}{16}\rho g H^2 (1+G) \tag{25}$$

$$S_p = \frac{1}{16}\rho g H^2 G \tag{26}$$

where $G = 2kh / \sinh 2kh$. Also, inside the surfzone, Eqs. (23) and (24) can be rewritten through the results of the roller used by Svendsen (1984).

$$S_m = \frac{1}{16}\rho g H^2 \frac{c^2}{gh}\left[B_0 + \frac{A}{H^2}\frac{h}{L}\right] \tag{27}$$

$$S_p = \frac{1}{2}\rho g H^2 B_0 \tag{28}$$

where A is the roller area and B_0 is the wave shape parameter defined by:

$$B_o = \frac{1}{T}\int_0^T \left(\frac{\eta}{H}\right)^2 dt \tag{29}$$

2.8 Wave-induced Mass Flux Model

Outside the surfzone, the wave volume flux is given by:

$$Q_{w\alpha} = B_0 \frac{gH^2}{C}\frac{k_\alpha}{k} \tag{30}$$

where $k_\alpha = (\cos\alpha_w, \sin\alpha_w)$ and is the wave number vector in direction x_α, and C is the phase velocity.

Inside the surfzone, the wave volume flux is given by Svendsen (1984):

$$Q_{w\alpha} = \frac{H^2 C}{h}\left(B_0 + \frac{Ah}{H^2 L}\right)\frac{k_\alpha}{k} \tag{31}$$

CHAPTER 3
Basic Equation for Circulation Model

The circulation model of this study uses the Quasi-3D model. The essential concept of the Quasi-3D model is a combination between the 1DH (One Horizontal Dimension) undertow model and the 2DH (Two Horizontal Dimension) circulation model, which was first developed by Van Dongeren et al. (1994) and has since been improved by Svendsen and Putrevu (1994, 1999). More details can be seen in their literature.

3.1 Separation of Currents

Svendsen and Putrevu (1999) split the instantaneous horizontal velocity $u_\alpha(x,y,z,t)$ into four components in order to consider the vertical variation of currents.

$$u_\alpha = u_\alpha^{\prime} + u_{w\alpha} + \bar{V}_\alpha + V_{1\alpha} \tag{32}$$

More recently, Svendsen (2005) used another notation for Equation (32) to comfortably derive equations, and it is as follows:

$$u_\alpha = u_\alpha^{\prime} + u_{w\alpha} + V_\alpha \tag{33}$$

where $u_\alpha^{\prime}$ is the turbulence component, $u_{w\alpha}$ is the wave component which is zero below the trough, and V_α is the short-wave-average velocity component, which represents the “current”.

3.2 Time-averaged and Depth-averaged Equations

The instantaneous mass flux of flow can be defined as:

$$M_\alpha = \int_{-h_o}^{\zeta} \rho u_\alpha dz \tag{34}$$

In considering simple continuity, the conservation of mass becomes the continuity equation as follows:

$$\frac{\partial(\rho_s \zeta)}{\partial t} + \frac{M_\alpha}{x_\alpha} = 0 \tag{35}$$

where ρ_s is the fluid density at the surface. In most of the studies on nearshore flows, fluid density is assumed to be constant, although density, such as reduced density due to bubbles in the turbulent behavior at the front of a breaking wave, is changed.

With ρ = const., the conservation of mass is equivalent to a conservation of volume. Hence volume flux Q_α can be defined as follows:

$$Q_\alpha = \int_{-h_o}^{\zeta} u_\alpha dz \tag{36}$$

The depth integrated continuity equation may therefore be written simply as:

$$\frac{\partial \zeta}{\partial t} + \frac{\partial Q_\alpha}{x_\alpha} = 0 \tag{37}$$

Also, the time average of Eq. (41) becomes:

$$\frac{\partial \overline{\zeta}}{\partial t} + \frac{\partial \overline{Q_\alpha}}{x_\alpha} = 0 \tag{38}$$

where $\overline{Q_\alpha}$ represents the total volume flux including the wave volume flux due to short wave motion.

In order to derive the depth integrated momentum equation, the term of the horizontal and vertical components of the momentum part of the Reynolds equations are introduced and are as follows:

$$\frac{\partial u_\beta}{\partial t} + \frac{\partial u_\alpha u_b}{x_\alpha} + \frac{u_\beta}{z} = -\frac{1}{\rho}\delta_{\alpha\beta}\frac{\partial p}{x_\alpha} + \frac{1}{\rho}\left(\frac{\partial \tau_{\alpha\beta}}{\partial x_\alpha} + \frac{\tau_{z\beta}}{z}\right) \quad \text{(Horizontal component)} \quad (39)$$

$$\frac{\partial w}{\partial t} + \frac{\partial u_\alpha w}{x_\alpha} + \frac{w^2}{z} = -\frac{1}{\rho}\frac{p}{z} - g + \frac{1}{\rho}\left(\frac{\partial \tau_{\alpha z}}{\partial x_\alpha} + \frac{\partial \tau_{zz}}{z}\right) \quad \text{(Vertical component)} \quad (40)$$

Eq. (39) is integrated over the water depth and partial differential operations can be moved from under the integration sign to the outside by using the Leibnitz rule. Through such processes, Eq. (39) can be written as:

$$\begin{aligned} &\rho\frac{\partial}{\partial t}\int_{h_0}^{\zeta} u_\beta dz + \rho\frac{}{x_\alpha}\int_{-h_o}^{\zeta} u_\alpha u_\beta dz = p(-h_0)\frac{\partial h_0}{x_\beta} + \\ &\frac{\partial}{\partial x_\alpha}\int_{-h_o}^{\zeta}\left(-p\delta_{\alpha\beta} + \tau_{\alpha\beta}\right)dz + R_\beta^S - \tau_\beta^B \end{aligned} \quad (41)$$

which is the instantaneous depth integrated horizontal momentum equation and is rewritten about time averaging:

$$\begin{aligned} &\rho\frac{\partial}{\partial t}\overline{\int_{h_0}^{\zeta} u_\beta dz} + \rho\frac{}{x_\alpha}\overline{\int_{-h_o}^{\zeta} u_\alpha u_\beta dz} = \overline{p(-h_0)}\frac{\partial h_0}{x_\beta} + \\ &\frac{\partial}{\partial x_\alpha}\overline{\int_{h_0}^{\zeta} -\delta_{\alpha\beta} p dz} + \frac{}{x_\alpha}\overline{\int_{-h_0}^{\zeta} \tau_{\alpha\beta} p dz} + \overline{R_\beta^S} - \overline{\tau_\beta^B} \end{aligned} \quad (42)$$

The vertical component, Eq. (40), is also integrated as follows:

$$p(z_0) = \rho g(\zeta - z_0) - \rho w \left(u_\alpha \frac{\partial z_0}{\partial x_\alpha} \right)_{z_0} + \frac{\partial}{\partial t} \int_{z_0}^{\zeta} \rho w dz + \frac{\partial}{\partial x_\alpha} \int_{z_0}^{\zeta} \rho u_\alpha w dz + \left(\tau_{\alpha z} - \tau_{\alpha z} \frac{\partial z_0}{\partial x_\alpha} \right)_{z_o} - \frac{\partial}{\partial x_\alpha} \int_{z_0}^{\zeta} \tau_{\alpha z} dz \tag{43}$$

and the stresses used in Eq. (43) are shown in Fig. 2.

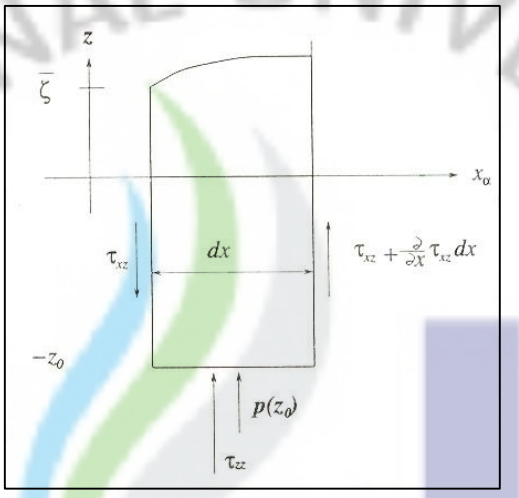

Fig. 2 Relation of the stresses on column of fluid (from Svendsen, 2005)

Through Eq. (43), the pressure $p(z)$ at an arbitrary depth can be obtained as follows:

$$p(z) = \rho g(\zeta - z) - \rho \left(\frac{1}{2} w^2 + \frac{1}{2} \hat{w}^2 \right) + \frac{\partial}{\partial t} \int_{z}^{\zeta} \rho w dz + \frac{\partial}{\partial x_\alpha} \int_{-z}^{\zeta} \rho \left(u_\alpha w + u_\alpha \hat{w} \right) dz \tag{44}$$

Also, the time averaged equation over the short wave period of Eq. (44) is as follows:

$$\overline{p(z)} = \rho g(\bar{\zeta} - z) - \rho \left(\frac{1}{2} \overline{w^2} + \frac{1}{2} \overline{\hat{w}^2} \right) + \frac{\partial}{\partial x_\alpha} \int_{-z}^{\zeta} \overline{\rho \left(u_\alpha w + u_\alpha \hat{w} \right)} dz \tag{45}$$

where $\hat{}$ means turbulent averaging.

By substituting $z = -h_0$ in the above Eq. (43) and using the bottom boundary condition, the pressure $p(z_0)$ at the bottom can also be obtained as follows:

$$p(-h_0) = \rho g(\zeta + h_0) + \frac{\partial}{\partial t}\int_{h_0}^{\zeta} \rho w dz + \frac{}{x_\alpha}\int_{-h_0}^{\zeta} \left(\rho u_\alpha w + \overline{u_\alpha w}\right) dz \tag{46}$$

The time averaged equation of Eq. (50) is as follows:

$$\overline{p(-h_0)} = \rho g(\bar{\zeta} + h_0) + \frac{\partial}{\partial x_\alpha}\int_{-h_0}^{\zeta} (\rho u_\alpha w + \tau_{\alpha z}) dz \tag{47}$$

Eq. (47), which is the term of the pressure at the bottom, is substituted into Eq. (42) and is mathematically solved on the right hand side. As a result, the time-averaged momentum equation is obtained as follows:

$$\begin{aligned} &\rho\frac{\partial}{\partial t}\int_{h_0}^{\zeta} u_\beta dz + \rho\frac{}{x_\alpha}\int_{-h_0}^{\zeta} u_\alpha u_\beta dz = -\rho g h\frac{\bar{\zeta}}{x_\beta} \\ &-\frac{\partial}{\partial x_\alpha}\int_{h_0}^{\zeta} \delta_{\alpha\beta} p dz - \delta_{\alpha\beta}\frac{1}{2}\rho g h^2 + \frac{}{x_\alpha}\int_{-h_0}^{\zeta} \tau_{\alpha\beta} dz + \overline{R_\beta^S} - \overline{\tau_\beta^B} \end{aligned} \tag{48}$$

By using Eq. (36), the relation between velocity and volume flux and by using Eq. (33), the separation of waves and currents, Eq. (48) can be derived, and the time-averaged, depth-integrated equation can then be obtained as follows:

$$\begin{aligned} &\rho\frac{\partial \bar{Q}_\beta}{\partial t} + \rho\frac{\partial}{\partial x_\alpha}\int_{h_0}^{\zeta} V_\alpha V_\beta dz + \rho\frac{}{x_\alpha}\int_{\zeta_t}^{\zeta} u_{w\alpha} V_\beta + u_{w\beta} V_\alpha dz = \\ &-\rho g(h_0 + \bar{\zeta})\frac{\partial \bar{\zeta}}{\partial x_\beta} - \frac{\partial}{\partial x_\alpha} S_{\alpha\beta} - \int_{-h_0}^{\zeta} \tau_{\alpha\beta} dz + \overline{\tau_\beta^S} - \overline{\tau_\beta^B} \end{aligned} \tag{49}$$

where $S_{\alpha\beta}$ is as follows:

$$S_{\alpha\beta} = S_{\alpha\beta} + \rho\frac{\overline{Q_{w\alpha} Q_{w\beta}}}{h} \tag{50}$$

Also, τ_β^S and τ_β^B are the surface and bottom shear stresses, respectively.

3.3 Solution for Separation of Currents

Substituting Eq. (33) into Eq. (36) yields the following equation:

$$Q_\alpha = \int_{-h_0}^{\zeta} (V_\alpha + u_{w\alpha} + u_\alpha')dz \tag{51}$$

Also, the ensemble and time averaged equation of Eq. (51) is as follows:

$$\overline{Q_\alpha} = \overline{\int_{-h_0}^{\zeta} (V_\alpha + u_{w\alpha})dz} \tag{52}$$

where turbulent component is assumed to be zero. In addition, because $u_{w\alpha}$, the wave component, is equivalent to zero below the trough, Eq. (52) leads to the following:

$$\overline{Q_\alpha} = \overline{\int_{h_0}^{\zeta} V_\alpha dz} + \overline{\int_{\zeta_t}^{\zeta} u_{w\alpha} dz} \tag{53}$$

The last term can introduce following definition:

$$Q_{w\alpha} = \overline{\int_{\zeta_t}^{\zeta} u_{w\alpha} dz} \tag{54}$$

Consequently, Eq. (53) can be written as follows:

$$\overline{Q_\alpha} = \overline{\int_{-h_0}^{\zeta} V_\alpha dz} + Q_{w\alpha} = V_\alpha h + Q_{w\alpha} \tag{55}$$

Eq. (49), the momentum equation, is written in terms of the total current velocity, V_α and a short-wave velocity, $u_{w\alpha}$. V_α, the total current velocity, may be divided into the current velocity by splitting it into a depth uniform part and a depth-varying part as follows:

$$V_\alpha(z) = V_{m\alpha} + V_{d\alpha}(z) \tag{56}$$

where the depth uniform component is defined by :

$$V_{m\alpha} \equiv \frac{\overline{Q_\alpha} - Q_{w\alpha}}{h} \tag{57}$$

Eq. (54) means that the depth uniform component of the current does not include the wave volume flux which is generated by wave behavior between crest and trough. And the combination of Eqs. (56) and (57) implies that $V_{d\alpha}$ is defined as follows:

$$\overline{\int_{h_0}^{\zeta} V_{d\alpha} dz} = 0 \tag{58}$$

Substituting Eq. (56) into Eq. (49) yields the following equation:

$$\frac{\partial \overline{Q_\beta}}{\partial t} + \frac{\partial}{\partial x_\alpha}\left(\frac{\overline{Q_\alpha Q_\beta}}{h}\right) + \frac{\partial}{\partial x_\alpha}\overline{\int_{h_0}^{\zeta} V_{d\alpha} V_{d\beta} dz} + \frac{\partial}{\partial x_\alpha}\overline{\int_{\zeta_t}^{\zeta} u_{w\alpha} V_{d\beta} + u_{w\beta} V_{d\alpha} dz} =$$
$$-g(h_0 + \overline{\zeta})\frac{\partial \overline{\zeta}}{\partial x_\beta} - \frac{1}{\rho}\frac{\partial}{\partial x_\alpha}\left(S_{\alpha\beta}\right) - \overline{\int_{h_0}^{\zeta} \tau_{\alpha\beta} dz} + \frac{\tau_\beta^S}{\rho} - \frac{\tau_\beta^B}{\rho} \tag{59}$$

3.4 Vertical Velocity Profiles

The solution for the vertical profiles of currents is essentially a generalization of the 1-DH undertow model and Eq. (59) need to be solved for this. The momentum equation given by Eq. (59) comprises of terms of depth-averaged properties except for the integral terms. In order to evaluate the integral terms, $V_{d\alpha}$, the depth varying component, should be derived. The following horizontal momentum equation is used to solve the problems:

$$\frac{\partial u_\alpha}{\partial t}+\frac{\partial u_\alpha u_\beta}{\partial x_\beta}+\frac{\partial u_\alpha w}{\partial z}=-\frac{1}{\rho}\frac{\partial p}{\partial x_\alpha}+\frac{1}{\rho}\left(\frac{\partial \tau_{\alpha\beta}}{\partial x_\beta}+\frac{\partial \tau_{\alpha z}}{\partial z}\right) \tag{60}$$

where p is the instantaneous pressure and is assumed hydrostatically as follows:

$$\overline{p}=\rho g\left(\overline{\zeta}-z\right) \tag{61}$$

In Eq. (60), the velocity separations are introduced into a wave and a current part and the following equation is then yielded:

$$\begin{aligned}
&\frac{\partial V_{d\alpha}}{\partial t}-\frac{\partial}{\partial z}\left(\left(\nu_t+\nu_s\right)\frac{\partial V_{d\alpha}}{\partial z}\right)=-\left(\frac{\partial \frac{\overline{Q}_\alpha}{h}}{\partial t}+\frac{\overline{Q}_\beta}{h}\frac{\partial \frac{\overline{Q}_\alpha}{h}}{\partial x_\beta}+g\frac{\partial \overline{\zeta}}{\partial x_\alpha}+f_\alpha\right)\\
&-\left(\frac{\overline{Q}_\beta}{h}\frac{\partial V_{d\alpha}}{\partial x_\beta}+V_{d\beta}\frac{\partial \frac{\overline{Q}_\alpha}{h}}{\partial x_\beta}+V_{d\beta}\frac{\partial V_{d\alpha}}{\partial x_\beta}+W\frac{\partial V_{d\alpha}}{\partial z}\right)\\
&+\left(\begin{array}{l}\frac{\partial \frac{Q_{w\alpha}}{h}}{\partial t}+\frac{\overline{Q}_\beta}{h}\frac{\partial \frac{Q_{w\alpha}}{h}}{\partial x_\beta}+\frac{Q_{w\beta}}{h}\frac{\partial \frac{\overline{Q}_\alpha}{h}}{\partial x_\beta}-\frac{Q_{w\beta}}{h}\frac{\partial \frac{Q_{w\alpha}}{h}}{\partial x_\beta}+\frac{Q_{w\beta}}{h}\frac{\partial V_{d\alpha}}{\partial x_\beta}\\ +V_{d\beta}\frac{\partial \frac{Q_{w\alpha}}{h}}{\partial x_\beta}\end{array}\right)\\
&+\frac{\partial}{\partial x_\alpha}\left(\left(\nu_t+\nu_s\right)\left(\frac{\partial V_\alpha}{\partial x_\beta}+\frac{\partial V_\beta}{\partial x_\alpha}\right)\right)+\frac{\partial}{\partial z}\left(\left(\nu_t+\nu_s\right)\frac{\partial W}{\partial x_\alpha}\right)
\end{aligned} \tag{62}$$

where f_α is as follows:

$$f_\alpha=\frac{\partial}{\partial x_\alpha}\left(\overline{u_{w\alpha}u_{w\beta}}\right)+\frac{}{z}\left(\overline{u_{w\alpha}w_w}\right) \tag{63}$$

Also, ν_t and ν_s are the eddy viscosity and the Smagorinksy eddy viscosity coefficients, respectively.

In Eq. (62), it is necessary for $V_{d\alpha}$ to be solved, whereby $V_{d\alpha}$ is divided into two parts as follows:

$$V_{d\alpha} = V_{d\alpha}^{(0)} + V_{d\alpha}^{(1)} \tag{64}$$

The vertical variation of $V_{d\alpha}^{(0)}$ is also written as follows:

$$V_{d\alpha}^{(0)} = d_{1\alpha}\xi^2 + e_{1\alpha}\xi + f_{1\alpha} + f_{2\alpha} \tag{65}$$

where $\xi = z + h_0$, $d_{1\alpha} = -\frac{F_\alpha}{2\nu_t}$, $e_{1\alpha} = \frac{\tau_\alpha^B}{\rho\nu_t}$, $f_{1\alpha} = -\frac{h}{2}\frac{\tau_\alpha^B}{\rho(\nu_t + \nu_s)}$, and $f_{2\alpha} = \frac{h^2 F_\alpha}{6(\nu_t + \nu_s)}$.

Also, F_α is given by:

$$F_\alpha = \left(\frac{1}{\rho h}\right)\frac{\partial S_{\alpha\beta}}{\partial x_\beta} - \frac{\tau_\alpha^S}{\rho h} + \frac{\tau_\alpha^B}{\rho h} - f_\alpha \tag{66}$$

In addition, $V_{d\alpha}^{(1)}$ is given by:

$$V_{d\alpha}^{(1)} = V_{d\alpha}^{(1,a)} + V_{d\alpha}^{(1,b)} + V_{d\alpha}^{(1,w)} + V_{d\alpha}^{(1,c)} \tag{67}$$

with

$$V_{d\alpha}^{(1,a)} = V_{d\alpha}^{(1,a,4)}\xi^4 + V_{d\alpha}^{(1,a,3)}\xi^3 + V_{d\alpha}^{(1,a,2)}\xi^2 \tag{68}$$

$$V_{d\alpha}^{(1,b)} = V_{d\alpha}^{(1,b,4)}\xi^4 + V_{d\alpha}^{(1,b,3)}\xi^3 + V_{d\alpha}^{(1,b,2)}\xi^2 \tag{69}$$

$$V_{d\alpha}^{(1,w)} = V_{d\alpha}^{(1,w,4)}\xi^4 + V_{d\alpha}^{(1,w,3)}\xi^3 + V_{d\alpha}^{(1,w,2)}\xi^2 \tag{70}$$

$$V_{d\alpha}^{(1,w)} = V_{d\alpha}^{(1,w,4)}\xi^4 + V_{d\alpha}^{(1,w,3)}\xi^3 + V_{d\alpha}^{(1,w,2)}\xi^2 \tag{71}$$

$$V_{d\alpha}^{(1,c)} = \begin{array}{l} \text{强烈推荐}\ V_{d\alpha}^{(1,a,4)} + V_{d\alpha}^{(1,b,4)} + V_{d\alpha}^{(1,w,4)}\ \frac{h^4}{5} \\ \text{强烈推荐}\ V_{d\alpha}^{(1,a,3)} + V_{d\alpha}^{(1,b,3)} + V_{d\alpha}^{(1,w,3)}\ \frac{h^3}{5} \\ \text{强烈推荐}\ V_{d\alpha}^{(1,a,2)} + V_{d\alpha}^{(1,b,2)} + V_{d\alpha}^{(1,w,2)}\ \frac{h^2}{5} \end{array} \tag{72}$$

3.5 Solution for the Integral Terms

The integral terms of Eq. (59) include current-current and current-wave interaction and they can be expressed in terms of the coefficients $M_{\alpha\beta}$, $D_{\alpha\gamma}$, $B_{\alpha\beta}$, and $A_{\alpha\beta\gamma}$ which are the 3D dispersion coefficients. To do this, the following approximations are introduced.

$$\overline{\int_{-h_0}^{\zeta} V_{d\alpha}\,dz} \approx \int_{-h_0}^{\bar{\zeta}} V_{d\alpha}\,dz \tag{73}$$

$$\overline{\int_{-h_0}^{\zeta} V_{d\alpha}V_{d\beta}\,dz + \int_{\zeta_t}^{\zeta} u_{w\alpha}V_{d\beta} + u_{w\beta}V_{d\alpha}\,dz} \approx \int_{-h_0}^{\bar{\zeta}} V_{d\alpha}V_{d\beta}\,dz \quad V_{d\beta}(\bar{\zeta})Q_{w\alpha} + V_{d\alpha}(\bar{\zeta})Q_{w\beta} \tag{74}$$

In the above equation, it is essentially assumed that $V_{d\alpha}$ remains constant between ζ_t and ζ, then the right hand side is approximately defined as follows by neglecting surface stresses.

$$\int_{-h_0}^{\bar{\zeta}} V_{d\alpha}V_{d\beta}\,dz + V_{d\beta}(\bar{\zeta})Q_{w\alpha} + V_{d\alpha}(\bar{\zeta})Q_{w\beta} = M_{\alpha\beta} + A_{\alpha\beta\gamma}\frac{\bar{Q}_\gamma}{h} - h\left\{D_{\gamma\beta}\frac{\partial}{\partial x_\gamma}\left(\frac{\bar{Q}_\alpha}{h}\right) + D_{\gamma\alpha}\frac{\bar{Q}_\beta}{h}\frac{\partial}{\partial x_\gamma} + B_{\alpha\beta}\frac{\bar{Q}_\gamma}{h}\frac{\partial}{\partial x_\gamma}\right\} \tag{75}$$

The 3D dispersion coefficients of Eq. (75) are defined by:

$$A_{\alpha\beta\gamma} = -\left[\int_{-h_0}^{\bar{\zeta}} \frac{1}{(\nu_t+\nu_s)}\left(\int_{-h_0}^{z} \frac{\partial V_{d\alpha}^{(0)}}{\partial x_\gamma} - \frac{\partial \frac{Q_{w\alpha}}{h}}{x_\gamma} - \frac{\partial h_0}{\partial x_\gamma}\frac{V_{d\alpha}^{(0)}}{z}\right)dz - \int_{-h_0}^{z} V_{d\beta}^{(0)} \frac{Q_{w\beta}}{h} dz\right]\right.$$
$$\left.\int_{-h_0}^{\bar{\zeta}} \frac{1}{(\nu_t+\nu_s)}\left(\int_{-h_0}^{z} \frac{\partial V_{d\beta}^{(0)}}{\partial x_\gamma} - \frac{\partial \frac{Q_{w\beta}}{h}}{x_\gamma} - \frac{\partial h_0}{\partial x_\gamma}\frac{V_{d\beta}^{(0)}}{z}\right)dz - \int_{-h_0}^{z} V_{d\alpha}^{(0)} \frac{Q_{w\alpha}}{h} dz\right] \tag{76}$$

$$B_{\alpha\beta} = -\frac{1}{h}\left[\int_{-h_0}^{\bar{\zeta}} \frac{1}{(\nu_t+\nu_s)}\left(\int_{-h_0}^{z} (h_0+z)\frac{\partial V_{d\alpha}^{(0)}}{z} dz\right)\right.$$
$$\left. - \int_{-h_0}^{z} V_{d\beta}^{(0)} \frac{Q_{w\beta}}{h} dz\right]$$
$$+\left[\int_{-h_0}^{\bar{\zeta}} \frac{1}{(\nu_t+\nu_s)}\left(\int_{-h_0}^{z} (h_0+z)\frac{\partial V_{d\beta}^{(0)}}{z} dz\right)\right. \tag{77}$$
$$\left. - \int_{-h_0}^{z} V_{d\alpha}^{(0)} \frac{Q_{w\alpha}}{h} dz\right]$$

$$D_{\alpha\beta} = \frac{1}{h}\left[\int_{-h_0}^{\bar{\zeta}} \frac{1}{(\nu_t+\nu_s)}\left(\int_{-h_0}^{z} V_{d\alpha}^{(0)} - \frac{Q_{w\alpha}}{h} dz\right) - \int_{-h_0}^{z} V_{d\beta}^{(0)} \frac{Q_{w\beta}}{h} dz\right] \tag{78}$$

$$M_{\alpha\beta} = \int_{-h_0}^{\bar{\zeta}} V_{d\alpha}^{(0)} V_{d\beta}^{(0)} dz + V_{dgb}^{(0)}(\bar{\zeta}) Q_{w\alpha} + V_{d\alpha}^{(0)}(\bar{\zeta}) Q_{w\beta} \tag{79}$$

3.6 Final Form of the Momentum and Continuity Equations

The final depth-averaged horizontal momentum equation is as follows:

$$\frac{\partial \bar{Q}_\alpha}{\partial t} + \frac{\partial}{\partial x_\alpha}\left(\frac{\overline{Q_\alpha Q_\beta}}{h}\right) + A_{\alpha\beta\gamma}\frac{\bar{Q}_\gamma}{h} + \frac{1}{\rho}\frac{\partial}{\partial x_\beta}\left(\int_{-h_0}^{\zeta}\tau_{\alpha\beta}dz\right) + \rho M_{\alpha\beta}$$
$$+ gh\frac{\partial \bar{\zeta}}{\partial x_\alpha} + \frac{\tau_\alpha^B}{\rho} - \frac{\partial}{\partial x_\beta}\left(\int_{-h_0}^{\zeta}\tau_{\alpha\beta}dz\right) + h\left(D_{\gamma\beta}\frac{\partial}{\partial x_\gamma}\left(\frac{\bar{Q}_\alpha}{h}\right) + D_{\gamma\alpha}\frac{\bar{Q}_\beta}{h}\right)\frac{\partial}{\partial x_\gamma}\left(\frac{\bar{Q}_\gamma}{h}\right) \quad (80)$$
$$- \frac{\partial}{\partial x_\beta}\left(hB_{\alpha\beta}\frac{\partial}{\partial x_\gamma}\left(\frac{\bar{Q}_\gamma}{h}\right)\right) = 0$$

and the x-momentum equation is as follows:

$$\frac{\partial Q_x}{\partial t} + \frac{\partial}{\partial x}\left(\frac{Q_x^2}{h}\right) + M_{xx}\frac{\partial}{\partial x}\left(\frac{Q_x Q_y}{h}\right) + M_{xy}\frac{\partial}{\partial y}$$
$$- \frac{\partial}{\partial x}h\left(2D_{xx} + B_{xx}\right)\frac{\partial}{\partial x}\left(\frac{Q_x}{h}\right) + 2D_{xy}\frac{\partial}{\partial y}\left(\frac{Q_x}{h}\right) + B_{xx}\frac{\partial}{\partial y}\left(\frac{Q_y}{h}\right)$$
$$- \frac{\partial}{\partial y}h\left(D_{xy} + B_{xy}\right)\frac{\partial}{\partial x}\left(\frac{Q_x}{h}\right) + D_{yy}\frac{\partial}{\partial y}\left(\frac{Q_x}{h}\right) + D_{xx}\frac{\partial}{\partial x}\left(\frac{Q_y}{h}\right) \quad (81)$$
$$+ \left(D_{xy} + B_{xy}\right)\frac{\partial}{\partial y}\left(\frac{Q_y}{h}\right) + \frac{\partial}{\partial x}\left(A_{xxx}\frac{Q_x}{h} + A_{xxy}\frac{Q_y}{h}\right) + \frac{\partial}{\partial y}\left(A_{xyx}\frac{Q_x}{h} + A_{xyy}\frac{Q_y}{h}\right)$$
$$= -gh\frac{\partial \bar{\zeta}}{\partial x} - \frac{1}{\rho}\frac{\partial}{\partial x}S_{xx} + \frac{\partial S_{xy}}{\partial y} + \frac{1}{\rho}\frac{\partial}{\partial x}\left(\int_{-h_0}^{\zeta}\tau_{xx}dz\right) + \frac{\partial}{\partial y}\left(\int_{-h_0}^{\zeta}\tau_{xy}dz\right) + \frac{\tau_x^S - \tau_x^B}{\rho}$$

then the y-momentum equation is as follows:

$$\frac{\partial Q_y}{\partial t} + \frac{\partial}{\partial x}\left(\frac{Q_x Q_y}{h}\right) + M_{xy}\frac{\partial}{\partial x}\left(\frac{Q_y^2}{h}\right) + M_{yy}\frac{\partial}{\partial y}$$
$$- \frac{\partial}{\partial x}h\left(D_{xy} + B_{xy}\right)\frac{\partial}{\partial x}\left(\frac{Q_x}{h}\right) + D_{yy}\frac{\partial}{\partial y}\left(\frac{Q_x}{h}\right) + D_{xx}\frac{\partial}{\partial y}\left(\frac{Q_y}{h}\right) + \left(D_{xy} + B_{xy}\right)\frac{\partial}{\partial y}\left(\frac{Q_y}{h}\right)$$
$$- \frac{\partial}{\partial y}h\left(B_{yy}\frac{\partial}{\partial x}\left(\frac{Q_x}{h}\right) + 2D_{xy}\frac{\partial}{\partial y}\left(\frac{Q_y}{h}\right) + \left(2D_{yy} + B_{yy}\right)\frac{\partial}{\partial y}\left(\frac{Q_y}{h}\right)\right) \quad (82)$$
$$+ \frac{\partial}{\partial x}\left(A_{xyx}\frac{Q_x}{h} + A_{xyy}\frac{Q_y}{h}\right) + \frac{\partial}{\partial y}\left(A_{xyy}\frac{Q_x}{h} + A_{yyy}\frac{Q_y}{h}\right)$$
$$= -gh\frac{\partial \bar{\zeta}}{\partial x} - \frac{1}{\rho}\frac{\partial}{\partial x}S_{xy} + \frac{\partial S_{yy}}{\partial y} + \frac{1}{\rho}\frac{\partial}{\partial x}\left(\int_{-h_0}^{\zeta}\tau_{xy}dz\right) + \frac{\partial}{\partial y}\left(\int_{-h_0}^{\zeta}\tau_{yy}dz\right) + \frac{\tau_y^S - \tau_y^B}{\rho}$$

and the continuity equation in x-y coordination is as follows:

$$\frac{\partial \bar{\zeta}}{\partial t} + \frac{Q_x}{x} + \frac{\partial Q_y}{y} = 0 \tag{83}$$

Eqs. (80), (81), (82), and (83) are used in the basic equation for circulation analysis.

3.7 Wind-induced Surface Shear Stress

In this study, the wind-induced surface stress is computed as follows:

$$\tau_\alpha^s = C_D \rho_\alpha |U| U_\alpha \tag{84}$$

where C_D is the drag coefficient, ρ_α is the air density and U is the wind velocity at 10m elevation above the ground. The drag coefficient is calculated from the formula proposed by the WAMDI group (Wave Modeling Group) (1988).

$$C_D = \begin{cases} 1.2875 \times 10^{-3} & U < 7.5 m/s \\ (0.8 + 0.065U) \times 10^{-3} & U \geq 7.5 m/s \end{cases} \tag{85}$$

CHAPTER 4
Model Implements

4.1 Numerical Scheme

4.1.1 Crank-Nicolson Technique

The parabolic model used in the wave analysis is conveniently solved in a finite difference form. In order to accomplish this, the analysis area must comprise a grid with x, y coordinates divided into rectangles of Δx and Δy sizes. The complex amplitude $A(x, y)$ will be found at each grid. The position of A by (i, j), where $x = (i-1)\mathrm{D}x$ and $y = (j-1)\mathrm{D}y$, can then be found. The difference scheme for the x-direction of a point located in (i, j) is defined as follows:

$$\frac{\partial A}{\partial x} = \frac{A_{i+1,j} - A_{i,j}}{\Delta x} \tag{86}$$

When $A_{i,j}$, $j = 1,2,3....n$, Eq. (86) can be solved directly for all the $A_{i+1,j}$. Therefore, the Crank-Nicolson scheme can be written as:

$$\begin{aligned} &aA_{i+1,j+1} + bA_{i+1,j} + cA_{i+1,j-1} \\ &= dA_{i,j+1} + eA_{i,j} + fA_{i,j-1} \end{aligned} \tag{87}$$

where the coefficient a, b, c, d, e, f involves variables of complex and nonlinear terms. Also, in this equation, the amplitudes at the left term are unknown, while the amplitudes at the right term are obtained through previous calculation. Through such process, the amplitudes are obtained from Eq. (87) and are used in Eq. (16).

4.1.2 Staggered Grid

For the circulation analysis, a staggered grid as shown in Fig. 3 is employed. In Fig. 3, the cross denotes the point at which ξ is computed, the circle denotes the point at which V_α^1 is computed and the square denotes the point at which V_α^2 is computed.

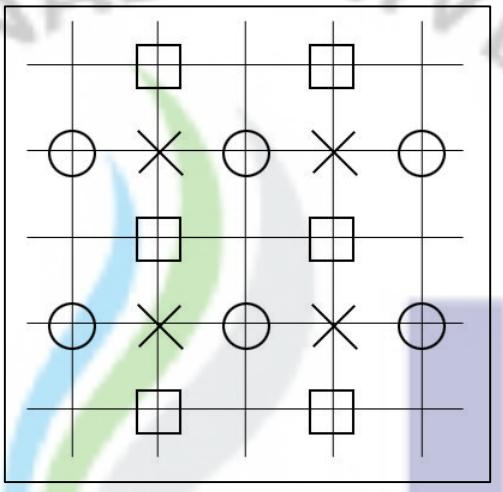

Fig. 3 Sketch grid in $\xi 1 - \xi 2$ plane

4.2 Boundary Conditions

Boundary conditions are very important problems for numerical analysis. There are several types of boundary conditions in the numerical model used in this study. First, the wall boundary condition can be used by Svendsen et al. (2004), in which the volume flux Q_α or ζ perpendicular to the boundary are set to zero. Second, the flux boundary added by the volume flux method is employed, which is used to deal with the in-out flux of inside or outside of flows along the boundary and defined as follows:

$$Q_\alpha = Q_\alpha^o \tag{88}$$

where Q_α is the depth-integrate and short-wave-averaged volume flux, and Q_α^o is the flux value at the boundary, which can be defined by the momentum and continuity equation about tide as follows:

$$Q_\alpha^o = \int_{-h_o}^{\zeta} u_t \, dz \tag{89}$$

where u_t means a velocity due to tidal oscillation and is defined as follows:

$$u_t = U_o \sin(\sigma t) \tag{90}$$

where U_o is the tidal amplitude and $\sigma = 2\pi / T$, T is the tidal period, and t is the time increment.

Third, a moving boundary condition for the shoreline in the domain of the model is employed, which uses the wet-dry method.

CHAPTER 5
Verification of the Numerical Model

To verify the numerical model of this study, verification models of two types are fulfilled. One verification model used in this study is compared to the results that had been observed by Watanabe and Maruyama (1984) and computed by Nishimura (1984). Another verification model is then also compared with the result obtained by Nishimura (1982).

5.1 Verification for Detached Break-water Case

The variations of the nearshore water flow in the sea area installed the detached breakwater were observed by Watanabe and Maruyama (1984). The experiment conditions for these studies are shown in Fig. 4, and the observation result is shown in Fig. 5.

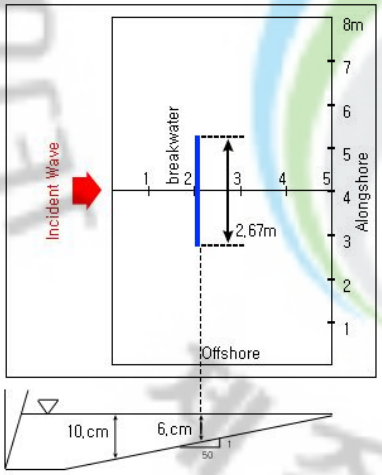

Fig. 4 Experiment set-up and coordinates (Watanabe and Maruyama, 1984)

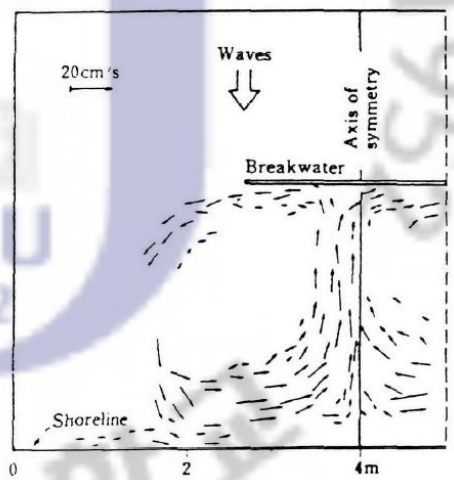

Fig. 5 Observed circulation identification (Watanabe and Maruyama, 1984)

A numerical analysis with the same conditions as Watanabe and Maruyama (1984) was then carried out by Nishimura (1984), and the results shown in Fig. 6 were compared with those shown in Fig. 5.

The observation and computation conditions have a seabed slope of $1:50$ and a constantly decreasing water depth. The detached breakwater of $2.67m$ is located in a fetch of $6m$ and a water depth of 6cm. In addition, the wave conditions are regular waves, the wave height $H_0 = 2cm$, and the period $T = 1.2\mathbf{sec}$. The incident wave angles are zero.

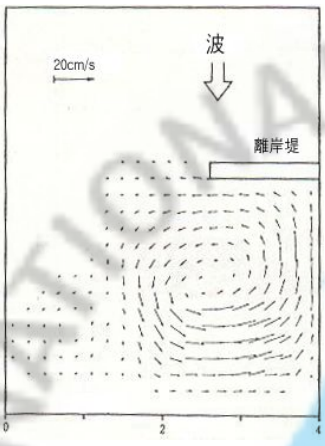

Fig. 6 Computed circulation result (Nishimura, 1984)

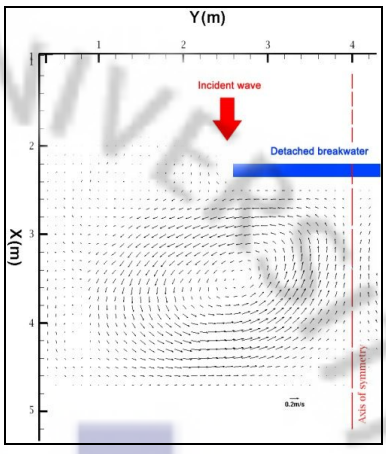

Fig. 7 Numerical result by this study

The open boundary condition is used as the boundary condition, and in order to compute a variation of flow at a shoreline, a moving boundary condition is applied to the detached breakwater and the shorelines. Such a moving boundary condition is implemented using a combined wet-dry method. In order to reduce the computation time, Δx and Δy, grid spaces used for the numerical analysis, are set at $10cm$. The time increment, Δt, is set at $0.02\mathbf{sec}$ so that wave-current interactions can be exactly considered. In order to correctly consider the steady flow through the numerical analysis, the computations are implemented over 2,000 periods.

The verification results of this study as shown in Fig. 7 are compared with those observed by Watanabe and Maruyama (1984) and computed by Nishimura (1984). The comparison shows good agreement between these results and those obtained in this study.

Examining the results of the verification model, it can be seen that strong vortex flows are generated behind the detached breakwater, which are nearly symmetrically circulated along the axis of symmetry of the detached breakwater. Such a phenomenon is also observed at a

real sea area installed the detached breakwaters. Therefore, sediments at a vicinity of the central area behind the detached breakwater are accumulated. Such results show that the nearshore currents are closely related to the refraction and diffraction of the waves.

5.2 Verification for Inclined Coast Case

As the next verification model, when incident waves attack an inclined coast, the numerical analysis for the nearshore current is carried out and compared with results obtained by Nishimura (1982). The numerical analysis conditions shown in Fig. 8 have the slope of $1:50$ in the seabed and a nearly constantly decreasing water depth, and the shoreline is inclined at $22.3°$ for the y-axis. Also, incident waves conditions are regular waves, the wave height $H_o = 4cm$, period $T = 0.64\sec$, and the incident wave angle $\theta = 0°$. The numerical analysis result obtained by Nishimura (1982) is shown in Fig. 9.

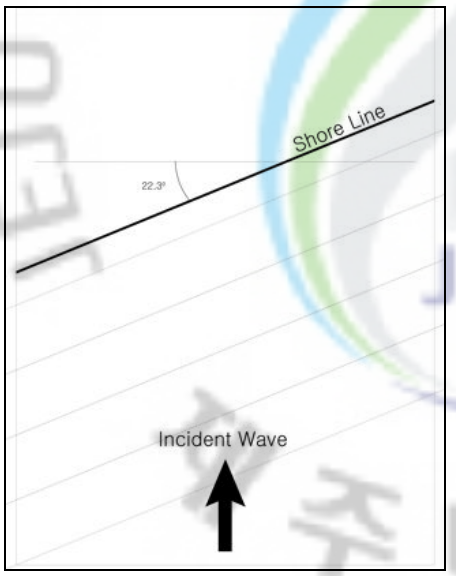

Fig. 8 Simulation Set-up and Coordinates (Nishimura, 1982)

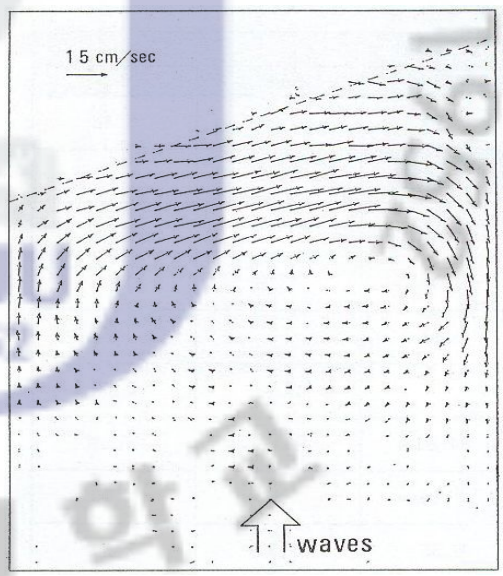

Fig. 9 Computed circulation result (Nishimura, 1982)

The numerical analysis result of this study is shown in Fig. 10. Also, the close boundary is used as the boundary condition, and a flow phenomenon is simulated at the inclined coast. In order to reduce the computation time, Δx and Δy, grid spaces used for the numerical

analysis, are set at $5cm$, respectively. The time increment, Δt, is set at $0.02\mathbf{sec}$ so that wave-current interactions can be considered exactly. After the computations are implemented for over 2,000 periods, the results of the computations are regarded as the steady flow.

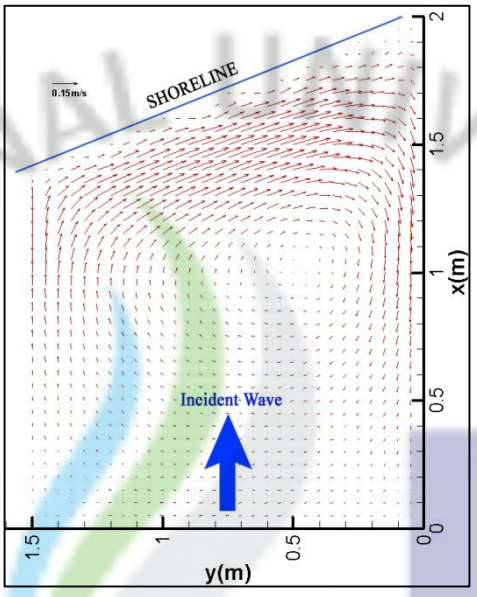

Fig. 10 Numerical Result by This Study

From a comparison between Fig. 9 and Fig. 10, it can be seen that the result of the numerical analysis in this study is in good agreement with results obtained by Nishimura (1982), and the existence of a rip current flowing out along the inclined coast is also confirmed.

CHAPTER 6
Model Applications

As the application of the numerical model, using the numerical model used in this study, circulation tendencies of the nearshore current on the real sea area are computed. These are performed as two types. One of these is a matter of variations of flows of the nearshore current, and another is how the wind-induced surface shear stresses act on flow. Study areas are Gangjeong Waters, Jeju and Haeundae Waters, Busan, respectively.

6.1 Simulation for Effects of Artificial Reefs

As first, in order to examine a variation of the nearshore current caused by artificial constructions, a flow tendency of the nearshore current in accordance with and without them in nearshore area is carried out.

The study area is Gangjeong located in Seoguipo, Jeju Island. It has a nearly mild slope sea bed, while there is a small rapidly sloped sea bed in part of the south area. Also, the analysis areas are the x-axis $=3.5km$ and y-axis $=2.8km$. A 3D bottom bathymetry of the study area is shown in Fig. 11.

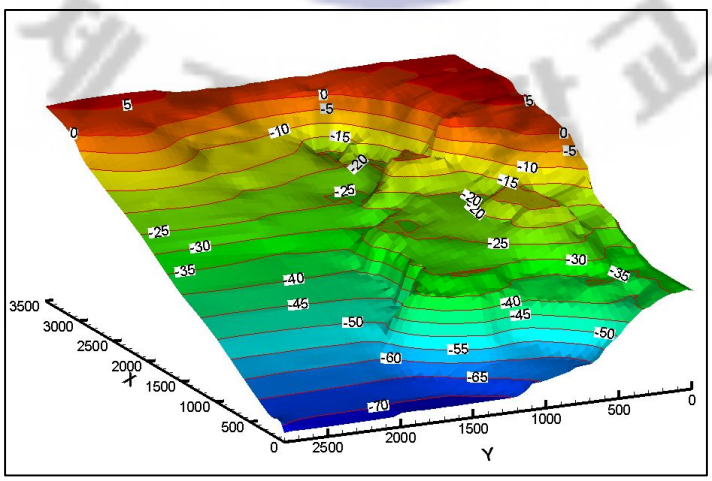

Fig. 11 3D bottom bathymetry in Gangjeong, Jeju Island

In the nearshore water circulation system, in order to examine that it is varied with artificial reefs, four types of applications are simulated. The first is the case without artificial reef, the second is the case with artificial reef at 20m water depth, the third is the case with artificial reef at 40m water depth, and the fourth is the case with artificial reefs at 20m & 40m water depth.

6.1.1 Numerical Analysis Conditions

From the first model applications, the numerical conditions are exactly the same in all types. The boundary conditions are the moving boundary, wall boundary, and flux boundary as mentioned in the above paragraph. Δx and Δy , the grid spaces, are set at 25m, the time increment Δt is 2.5sec and the wave conditions are $H_{1/3} = 1.5m$ and $T_{1/3} = 14\mathbf{sec}$, respectively. The numerical analysis is started as Cold Start, results of the computations after 2,000 periods are considered as the steady flow, and a total of 35,560 periods are computed. The plotting times of results are 1hour, 5hours, 9hours, and 13hours.

6.1.2 The Case without Artificial Reefs

To examine a variation of flow caused by artificial reefs, the tendency to water circulation without artificial reefs should be researched. A 3D bottom bathymetry of this case is already shown in Fig. 11.

From the numerical results of the surface velocity shown in Fig. 12 to Fig. 15, local vortices and the longshore currents caused by incident wave along the shorelines can be confirmed. And the rip current by an interaction of the longshore current between the North and South direction can be also confirmed. In particular; because the rock area exists in Gangjeong, it is shown that the refraction and diffraction of flows are generated by rock area.

The results of bottom velocities are shown in Fig. 16 to Fig.19, and they show a similar tendency to those of the surface velocity. However, the flows in the vicinity of a shoreline with the shallow water depth are somewhat changed. Such variations of bottom flows are especially generated in the area where longshore currents are separated to the North and South directions at the shoreline, where the flowing direction of the longshore current on the bottom due to such variations differ in surface flows.

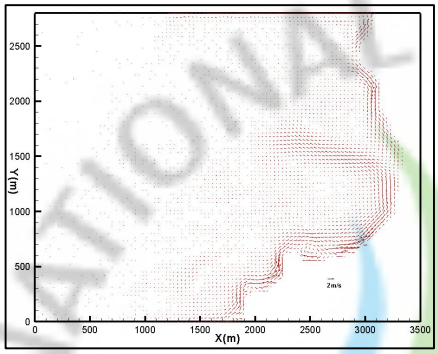

Fig. 12 Surface velocity (1hour)

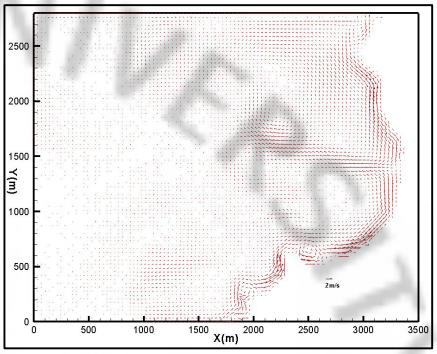

Fig. 13 Surface velocity (5hour)

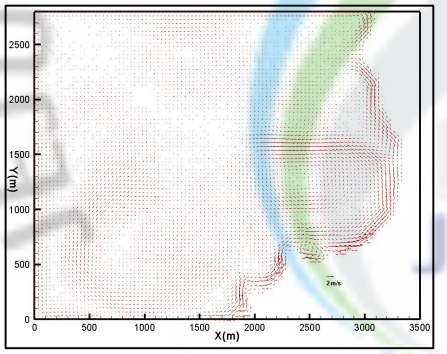

Fig. 14 Surface velocity (9hour)

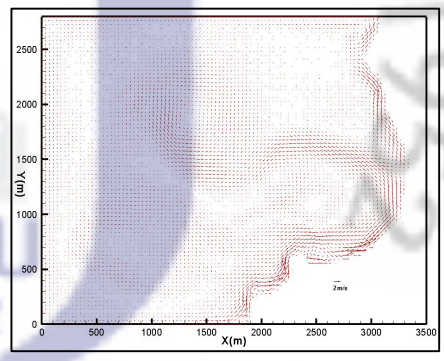

Fig. 15 Surface velocity (13hour)

In the results of the numerical simulations of wave height distribution shown in Fig. 20 to Fig. 23, it can be seen that the wave set-up phenomenon in the rock area where exists at south area are generated. The cause of such a wave set-up is the sudden changes to the water depths at the rock area, and this is also regarded as the cause for the refraction and the diffraction of flows. Consequently, because of the refraction and diffraction of flows, local strong vortices are generated behind the rock area. It is therefore clearly demonstrated that wave-current interactions are very important factors in nearshore current behavior.

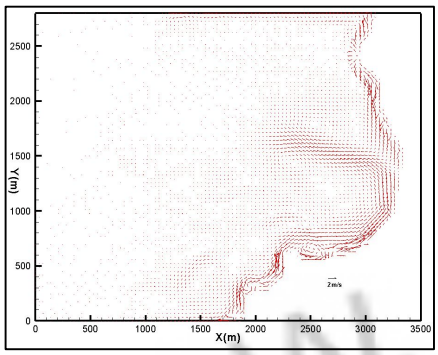

Fig. 16 Bottom velocity (1hour)

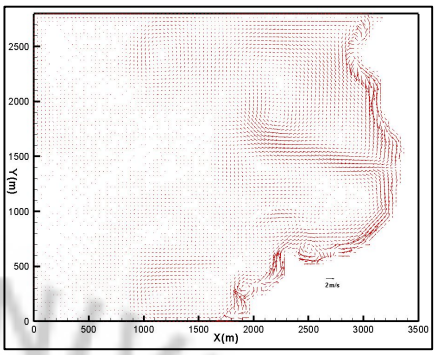

Fig. 17 Bottom velocity (5hour)

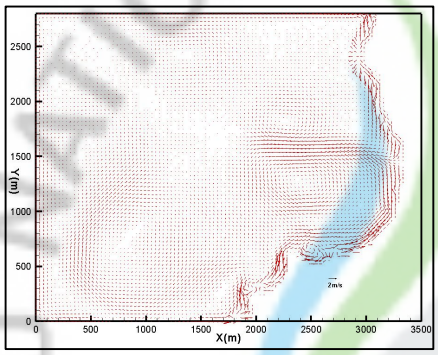

Fig. 18 Bottom velocity (9hour)

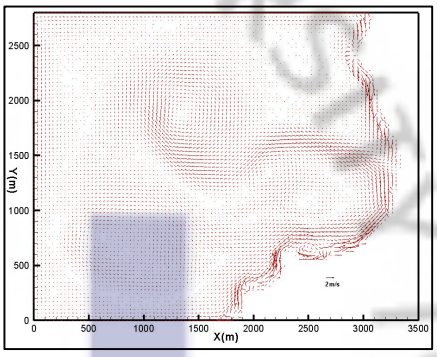

Fig. 19 Bottom velocity (13hour)

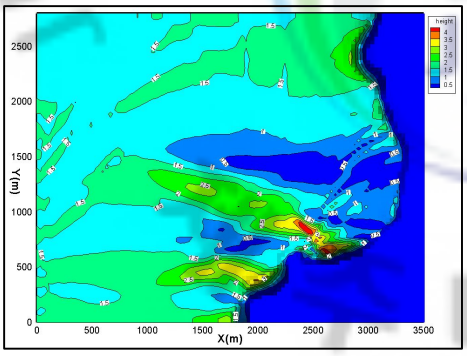

Fig. 20 Wave height distribution (1hour)

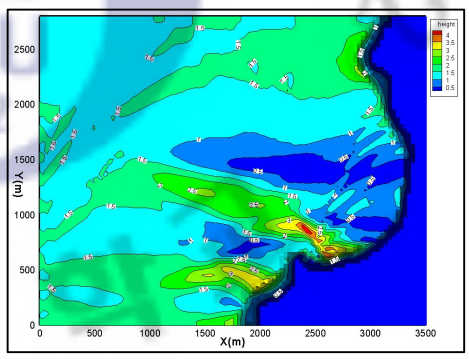

Fig. 21 Wave height distribution (5hour)

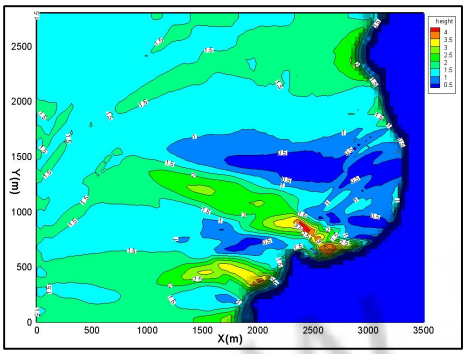

Fig. 22 Wave height distribution (9hour)

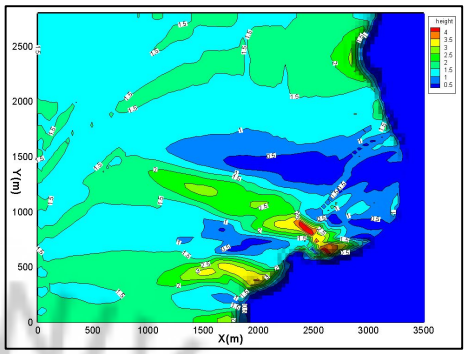

Fig. 23 Wave height distribution (13hour)

6.1.3 The Case with Artificial Reefs at 20m Water Depth

In this case, artificial reef is installed at a 20m water depth as shown Fig. 24. Those are comprised of impermeable square block reefs as shown in Fig. 25, and the dimensions are length=30m, height=8m, and width=8m. Surface velocity and wave distribution results of this case are similar to the case without these. In order to see a variation of the bottom flow due to artificial reef in detail, flows in the vicinity of these are only plotted.

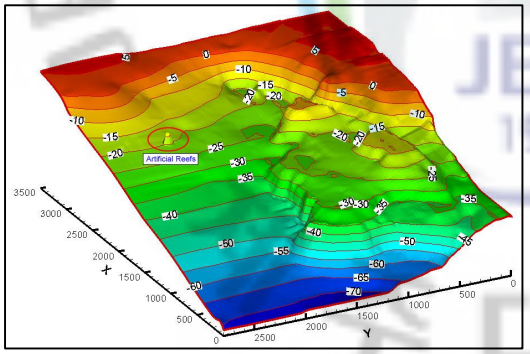

Fig. 24 3D bottom bathymetry of the case installed at a 20m water depth

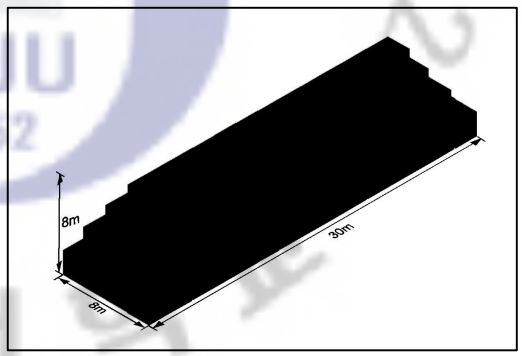

Fig. 25 3D sketch of the impermeable artificial reef

From the numerical results of this case shown in Fig. 26 to Fig. 29, the points denoted by A, B, C, and D represent areas where vortices are generated by artificial reef. Table 1 shows the values of velocity at each point.

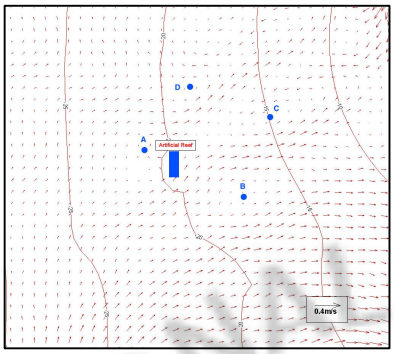

Fig. 26 Bottom velocity of case 2 (1hour)

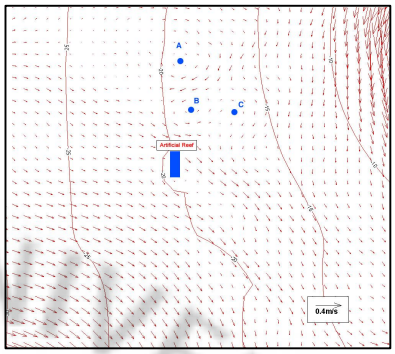

Fig. 27 Bottom velocity of case 2 (5hour)

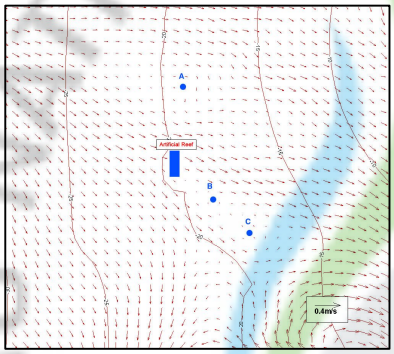

Fig. 28 Bottom velocity of case 2 (9hours)

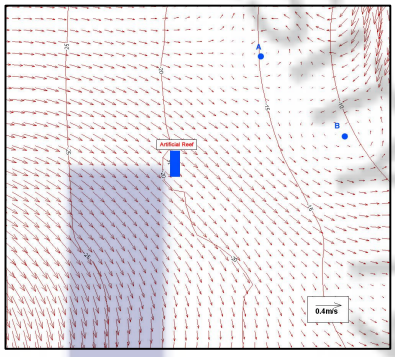

Fig. 29 Bottom velocity of case 2 (13hours)

Table 1 Values of local vortices in the vicinity of the artificial reef at a 20m water depth

	1hour	5hours	9hours	13hours
	Velocity(m/s)	Velocity(m/s)	Velocity(m/s)	Velocity(m/s)
A	0.01 ~ 0.012	0.016 ~ 0.02	0.015 ~ 0.018	0.027 ~ 0.03
B	0.009 ~ 0.015	0.013 ~ 0.015	0.01 ~ 0.012	0.002 ~ 0.08
C	0.0 1~ 0.02	0.014 ~ 0.017	0.01 ~ 0.013	
D	0.016 ~ 0.018			

6.1.4 The Case with Artificial Reef at 40m Water Depth

The results of the case where artificial reef is installed at a 40m water depth as shown in Fig. 30 are also plotted in the vicinity of those shown in Fig. 31 to Fig. 34, and table 2 shows the values of velocity.

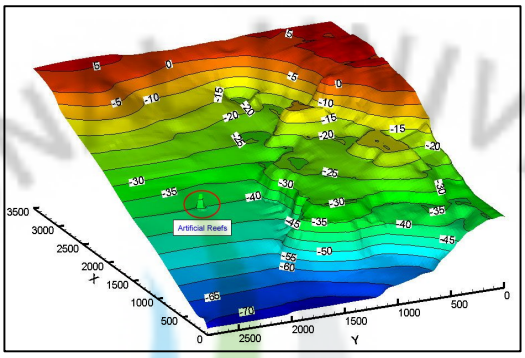

Fig. 30 3D bottom bathymetry of the case installed at a 40m water depth

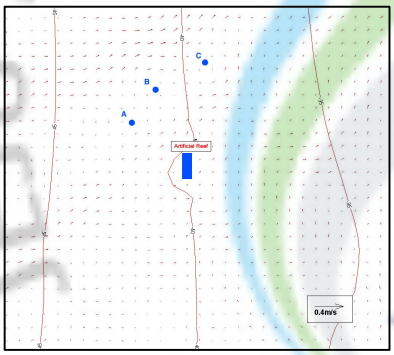

Fig. 31 Bottom velocity of case 3 (1hour)

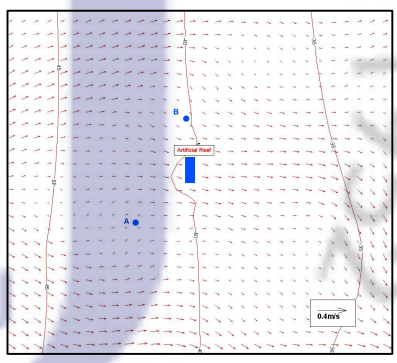

Fig. 32 Bottom velocity of case 3 (5hours)

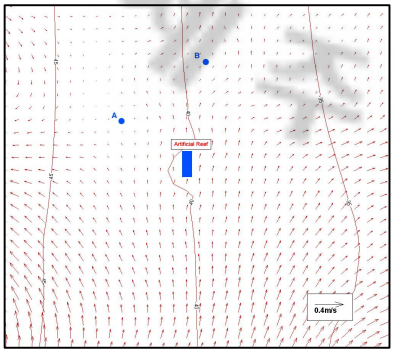

Fig. 33 Bottom velocity of case 3 (9hours)

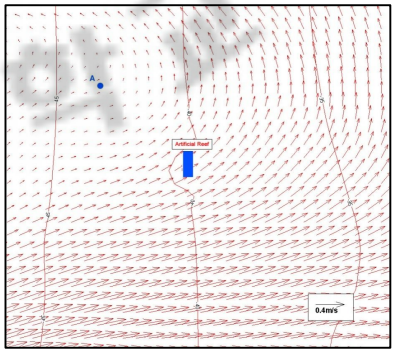

Fig. 34 Bottom velocity of case 3 (13hours)

Table 2 Values of local vortices in the vicinity of the artificial reef at a 40m water depth

	1hour	5hours	9hours	13hours
	Velocity(m/s)	Velocity(m/s)	Velocity(m/s)	Velocity(m/s)
A	0.0037 ~ 0.0043	0.0037 ~0.0043	0.0035 ~0.0042	0.003 ~ 0.004
B	0.0033 ~ 0.0037	0.0041~ 0.093	0.0038 ~ 0.0041	
C	0.0034 ~ 0.0041		0.01 ~ 0.013	

6.1.5 The Case with Artificial Reefs at 20m & 40m Water Depth

In order to examine the variation of water circulation due to the arrangement of artificial reefs, the case in which are installed at 20m & 40m water depth simultaneously is carried out. A bathymetry of this case is shown in Fig. 35. The results of this case are plotted as for the above case. These are shown in Fig. 36 to Fig. 39, and table 3 shows the values of velocity.

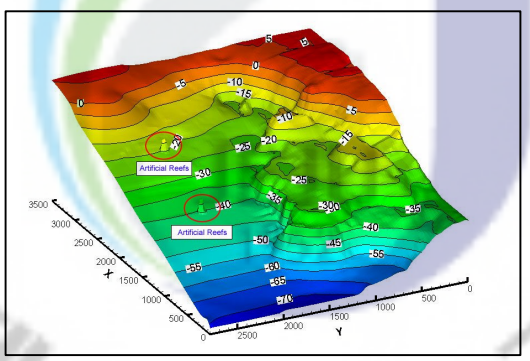

Fig. 35 3D bottom bathymetry of the case installed at 20m & 40m water depths simultaneously

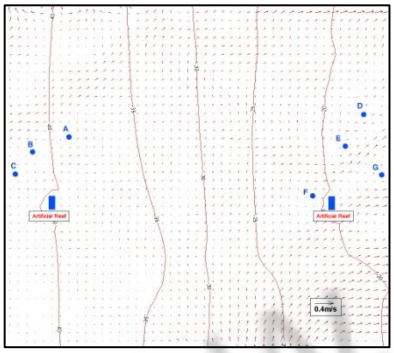

Fig. 36 Bottom velocity of case 3 (1hour)

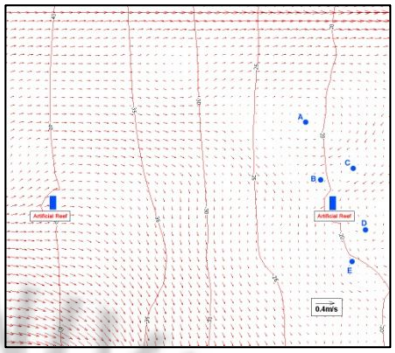

Fig. 37 Bottom velocity of case 3 (5hours)

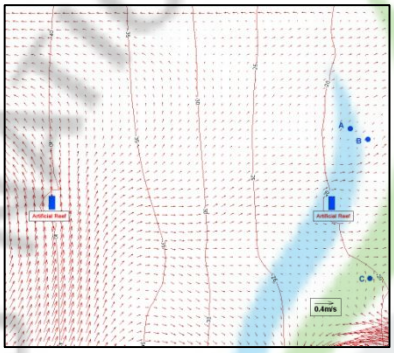

Fig. 38 Bottom velocity of case 3 (9hours)

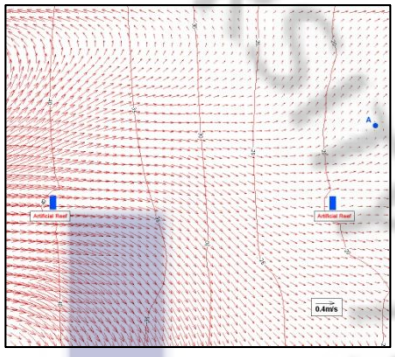

Fig. 39 Bottom velocity of case 3 (13hours)

Table 3 Values of local vortices in the vicinity of the artificial reef at 20m & 40m water depths

	1hour	5hours	9hours	13hours
	Velocity(m/s)	Velocity(m/s)	Velocity(m/s)	Velocity(m/s)
A	0.004 ~ 0.006	0.009 ~ 0.014	0.018 ~ 0.021	0.018 ~ 0.024
B	0.001 ~ 0.0035	0.01 ~ 0.013	0.019 ~ 0.022	
C	0.001 ~ 0.0043	0.0002 ~ 0.012	0.007 ~ 0.01	
D	0.01 ~ 0.017	0.012 ~ 0.014		
E	0.016 ~ 0.018	0.008 ~ 0.01		
F	0.0001 ~ 0.01			
G	0.016 ~ 0.02			

6.2 Simulation for Influence of Wind-induced Stress

As second application, the variations of the nearshore current caused by the wind stress at Haeundae beach are simulated. The influences of the wind on the water circulation within nearshore area are great. However, most of studies on these phenomena have not considered the influence of the wind. Therefore, in this study, the wind-induced surface shear stresses are examined how those occasion the variation of flows.

6.2.1 Numerical Analysis Conditions

In order to examine that circulation phenomena of water are varied as the wind-induced stress, the numerical model used in this study is applied to Haeundae Waters. A 3D bottom bathymetry of the study area is shown in Fig. 40. The analysis fields are x-axis = $3.7km$ and y-axis = $3.6km$, respectively. The wave data is taken from Lee, Tac and Woo (2007) and the wind data is taken from AWS (Automatic Weather Station). Lee, Tac and Woo (2007) yielded the wave data at Haeundae Waters for each season by analyzing wave data from 1979 to 2002. In this study, numerical analysis for the wave condition of summer among four seasons is carried out. The wind data used in the numerical analysis is velocity $5.9m/s$ and direction NE, and the wind direction is calculated as clockwise relative to y-axis. The grid spaces, Δx and Δy, are $50m$ by $50m$, and the time increment, Δt, is $2.0\,\mathbf{sec}$. And the wave conditions are $H_{1/3} = 1.42m$ and $T_{1/3} = 8.0\,\mathbf{sec}$, and the incident direction is zero relative to x-axis.

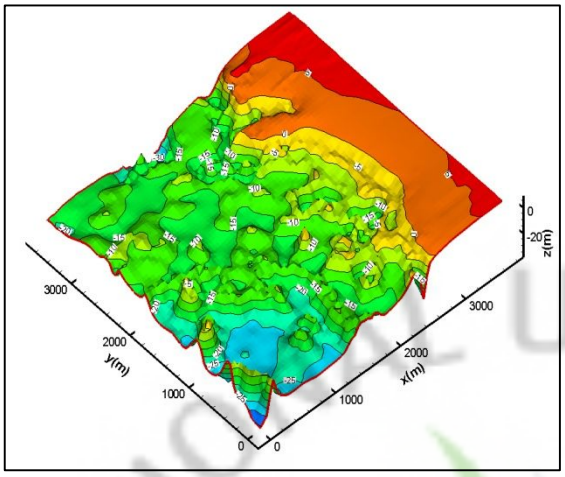

Fig. 40 3D bottom bathymetry in Haeundae waters, Busan

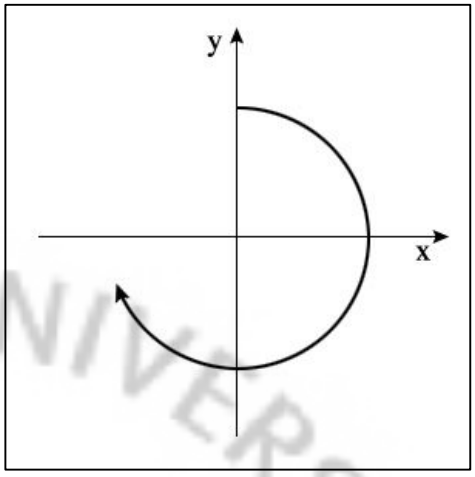

Fig. 41 Sketch definition of wind direction

6.2.2 Results of Numerical Model

By considering the wind-induced stress, surface elevation and velocity are varied. In order to see such variations, the numerical results are plotted for 2hour, and 5hour. From Fig. 42 to Fig. 45, these are results of surface elevation with or without the wind stress.

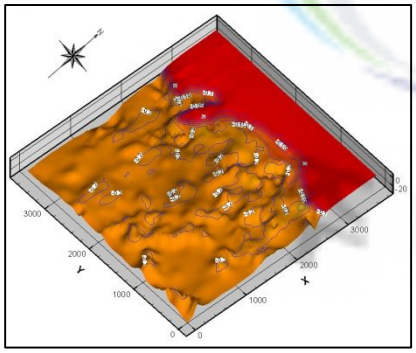

Fig. 42 Surface elevation at 2 hours without wind-induced stress

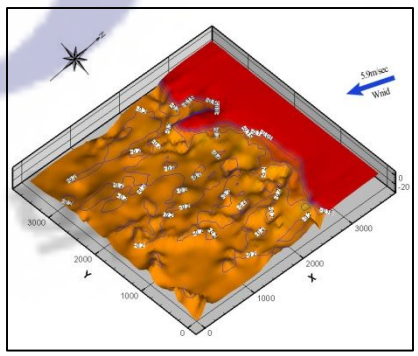

Fig. 43 Surface elevation at 2 hours with wind-induced stress

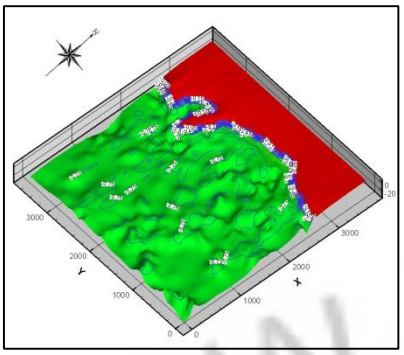

Fig. 44 Surface elevation at 5 hours without wind-induced stress

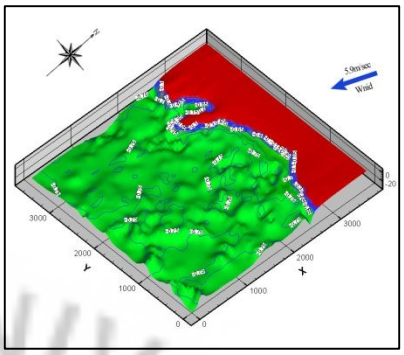

Fig. 45 Surface elevation at 5 hours with wind-induced stress

For results of surface velocity, these are also plotted as surface elevations, and are From Fig. 46 to Fig. 49.

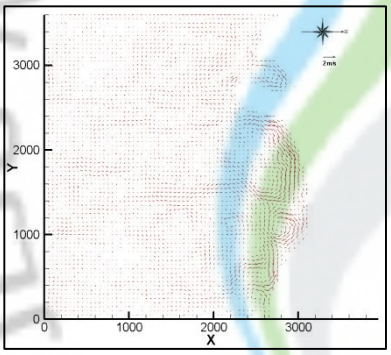

Fig. 46 Surface velocity at 2 hours without wind-induced stress

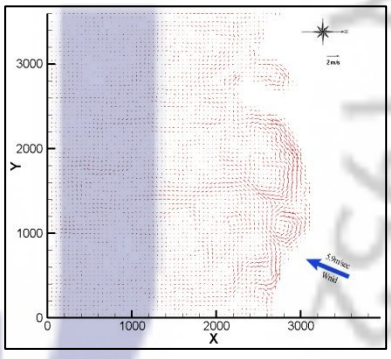

Fig. 47 Surface velocity at 2 hours with wind-induced stress

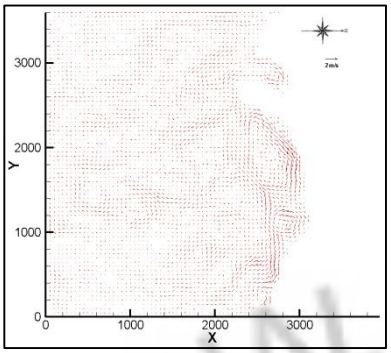

Fig. 48 Surface velocity at 5 hours without wind-induced stress

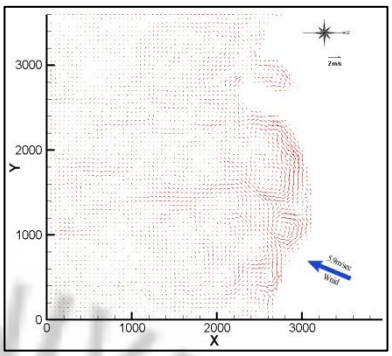

Fig. 49 Surface velocity at 5 hours with wind-induced stress

CHAPTER 7
Conclusions and Remarks

7.1 Conclusions and Remarks

In this study, the numerical model of the nearshore current considering nonlinear combined refraction-diffraction and vertical non-uniformity of flows is carried out. The parabolic mild slope equation and the Quasi-3D equation are applied to the numerical simulation used in this study. For the wave analysis, the parabolic mild slope equation and the Crank-Nicolson method are used. Consequently, more computation time can be saved than in the Boussinesq models. Also, for the circulation analysis, the Quasi-3D equation is used, and so the vertical non-uniformity of flows can be considered. In addition, the flux boundary condition is added by the volume flux method. Thus, a more exact computation for the circulation phenomenon can be computed exactly. By using the ADI method, the computation process is also efficient.

To verify the numerical model used in this study, the results from the verification model are compared with those observed by Watanabe and Maruyama (1984) and computed by Nishimura (1984, 1982). The comparisons show good agreement among these models.

In order to apply the numerical model used in this study to circulation phenomena at real sea area, numerical models about several conditions such as normal condition, condition established artificial constructions, and condition acting the wind-induced stresses are carried out, for the nearshore current may be varied with various factors. The condition established artificial constructions such as submerged breakwater and detached breakwater should be examined whether effects of them are corresponded with their purpose or how tendencies of flows are changed by them. And the wind-induced surface shear stresses affect the flow so these should be considered to perform more exact numerical analysises.

Seeing the results of the numerical model with artificial reefs or not, it can be seen that, because refraction and diffraction by the various bottom slope conditions occurred, the

nearshore circulation phenomena are varied. These results clearly indicate that circulation characteristics of the nearshore currents closely relate to refraction and diffraction of flows. In the numerical results of all cases, artificial vortices are generated by artificial reefs, and this is regarded as corresponding to purpose of them.

From each case, it can be seen that surface velocities and wave height distributions are almost similar, flow tendencies, however, in the vicinity of the bottom, the artificial reefs are installed at, are very different. In particular, by comparing case installed at 20m or 40m water depth by themselves with case installed at 20m and 40m water depth simultaneously, it can be seen that the latter case generates vortices more lively than the former case. This clearly shows that flow variations on bottom are closely associated with bottom shape. Also, in comparing case installed at 20m with 40m, respectively, the former is better for generating vortices than the latter. This is considered as for the latter is even more influenced by incident wave than the former and local vortices in the former are more lively generated by interacting with rip current flowing out from coast than the latter.

Next, examining the result of numerical model considering the wind force at Haeundae Waters, it can be seen that the surface elevations and velocities are varied with the winds against the incident wave direction. Such results comprehend that the water circulation phenomena may be changed by winds and it may cause various problems related to coastal engineering. To predict such potential problems and to solve these, studies on flow variation caused by the wind-induced stress should be persistently performed.

Through the numerical model used in this study, flow tendencies of the nearshore on normal condition can be predicted, and further, studies on accumulations and erosions problems due to sediment transport can be fulfilled. Also, flow variations that may occur by a variety of factors such as artificial constructions and wind-induced stresses can be predicted. By standing on researches carried out in this study, it can be considered that these studies contribute to developing and utilizing the nearshore regions effectively.

7.2 Future Works

The study fields, which need to be conduct in future, are listed below.

1. The present study does not include the model for the sediment transport. The numerical model for quantitative analysis of the sediment transport caused by the nearshore current should be established.

2. In order to conduct large-scale numerical models, the study on composing the non-orthogonal structured grid by using curve mesh generation method is also necessary, for the present numerical models through orthogonal structure grid are limited for computation time.

3. Computing the wind-induced stresses, the present model cannot consider the change of direction and speed of the wind, but these variations should be considered to perform more exact numerical model.

References

Berkhoff, J.C.W., 1972. Computation of combined Refraction-Diffraction, Proc.13 Coastal Eng. Conf., ASCE, pp. 471-490.

Birkemeir, W.A and R.A Dalrymple, 1976. Numerical models for the Prediction of Wave set up and Nearshore circulation, Ocean Eng. Rep., No. 3, Univ. Dalaware, Dept. of Civil Eng.

Booji, N., 1983. A note on the accuracy of the mild-slope equation, Coastal Engineering, vol 7, pp. 191-203.

Copeland, G.J.M., 1985. Numerical Model for the Propagation of Short Gravity Wave and the Resulting Circulation around Nearshore Structures, Ph. D. Dissertation, Univ. of Liverpool.

Longuet-Higgins, M.S. and Stewart, R.W., 1964. Radiation Stresses in Water Waves; a Physical Discussion, with Application, Deep-Sea RES., Vol 11, No. 4, pp. 529-562.

Sonu,C,j, 1972. Field Observation of Nearshore Circulation and Meandering Currents, J. of Geophy. Res., vol. 77, No. 18, pp. 3232-3247.

Liu, P.L.-F. and Mei, C.C, 1976. Water Motion on a Beach in the Presence of a Breakwater, 1 Waves, 2 Mean Currents, J. of Geophysical Res., Vol 81, pp. 3079-3085.

Kirby,J,T., 1986. Rational approximations in the parabolic equation method for water waves, Coastal Engineering, 10, 355-378.

Shepard, F .P. and Inman, D.L., 1950. Near shore Circulation Related to Bottom Topography and Wave Refraction, Trans . A m . Geophs . Union Vol 31 No. 4, pp. 555- 565.

Fengyan Shi, James T. Kirby, Daniel M. Hanes, 2007. An efficient mode-splitting method for a curvilinear nearshore circulation model, Coastal Engineering, Vol 54, pp. 811-824.

Putrevu, U., Svendsen, I.A., 1994. Nearshore mixing and dispersion, Proc. Roy. Soc. Lond A 445, pp. 567-576.

Putrevu, U., Svendsen, I.A., 1999. Three-dimensional dispersion of momentum in wave-induced nearshore currents, Eur. J . Mech. B, Fluids 18, pp. 83-101.

Svendsen, I.A., 2005. Introduction to nearshore hydrodynamics, Advanced Series on ocean Engineering, Vol.24, World Scientific.

Svendsen, I. A., Haas, K., and Zhao, Q., 2004. Quasi-3D Nearshore Circulation Model SHORECIRC: Version 2.0, Research Report, Center for Applied Coastal Research, University of Delaware.

Min, B. H., Lee, S. H., and Kim, I. C., 1991. A study the numerical model of wave induced current around nearshore structure, KSOE Journal of Ocean Engineering, Vol 5, No. 1, pp. 55-63.

Lee, J. M., Kim, J. J., and Park, J. C., 1998. A study the numerical models of wave induced, KSOE Journal of Ocean Engineering, Vol 12, No. 3, pp. 75-81.

Ham, G. U., Park, J. I., and Ahn, G. M., 1998. Analysis on Characteristics of Wave-Induced Current of Sangju Beach, KSCE Journal of Civil Engineering, Vol 22, No. 2-B, pp.171-180.

Nishimura, H., 1982. Numerical simulation of the nearshore circulation, Proc. 29th Japanese Conf. on Coastal Eng., JSCE, pp. 171-180.

Nishimura, H., 1984. About numerical simulation method of the nearshore circulation, Proc. 31th Japanese Conf. on Coastal Eng., JSCE, pp. 394-400.

Watanabe, A., and Maruyama, Y. T., 1984. Numerical analysis of the damping of breaking waves, including refraction diffraction, Proc. 31th Japanese Conf. on Coastal Eng., JSCE, pp. 103-107.

감사의 글

우선, 이 논문을 완성 할 수 있도록 2 년간의 대학원 생활 동안 끊임없는 사랑과 배려로 지도해주시고, 여러 가지로 부족한 제자에게 항상 변함없는 조언과 애정 어린 질책으로 석사과정을 무사히 마칠 수 있도록 보살펴 주신 김남형 교수님께 진심으로 감사 드립니다. 항상 교수님께서 건강히 후학을 양성 하실 수 있기를 기원 드립니다. 또한, 바쁘신 와중에서도 논문 심사를 맡으셔서 세심한 지도를 해 주신 김상진 교수님과 허영택 박사님께도 진심으로 감사를 드립니다. 지난 2 년 동안 학문적인 기초를 마련해주신 양성기 교수님, 남정만 교수님, 이병걸 교수님, 박상렬 교수님, 이동욱 교수님께도 진심으로 감사를 드립니다.

2 년간의 대학원 생활 동안, 같은 공간에 있다는 것만으로 나에게 큰 위안이 되어 주었던, 같은 연구실 동기이자 후배들인 창림이와 현철이에게 큰 고마움을 전합니다. 항상, 모자란 선배를 대신 하여 궂은일을 묵묵히 해주는 그들이 있었기에 대학원생활 동안 큰 어려움 없이 학업에 열중 할 수 있었던 것 같습니다. 창림이와 현철이도 원하는 모든 일들이 순조롭게 이루어 질 수 있기를 간절히 바랍니다.

1 학기 신입생 때부터, 모르는 것이 있을 때마다 찾을 수 밖에 없었던 행식형, 지원이, 향혜에게도 고마움을 전하고 싶습니다. 모르는 것이 있을 때 마다, 힘든 일이 있을 때 마다, 항상 친절하게 가르쳐 주고 조언을 아끼지 않았던 그들이 있었기에 큰 어려움 없이 2 년간의 석사과정을 무사히 마칠 수 있었습니다.

그리고, 가끔씩 찾아와서 오빠, 형 하면서 애교를 부리는 우리 학부생들, 정운이, 수민이, 주경이, 서리, 수진에게도 고마움 마음을 전합니다. 공부라는 어려운 길을 택한 후배들의 앞날에도 좋은 일만 가득하길 빕니다.

연구를 진행함에 있어서, 여러 가지 조언을 아낌없이 전해주신 허영택 선배님, 강현우 선배님, 양순보 선배님, 민수형, 경보형, 강일형 에게도 이 자리를 통해서 감사의 마음을 전하고 싶습니다. 저보다 먼저 경험을 하셨기에 한마디 한마디가 가슴 속에 깊게 전해지는 말씀들을 들으면서 약해지는 마음을 다잡을 수 있었던 것 같습니다.

그리고 비록 타 연구실이지만 대학원 생활을 같이하며 서로 의지가 되어준, 용현이, 태건이, 창선이, 영민이, 정우 에게도 고마움을 전하고 싶습니다. 어디에서 무엇을 하던 꼭 그들이 원하는 모든 일이 순조롭게 이루어지길 빕니다.

또한, 항상 막내 아들을 걱정하시는 부모님께 감사 드리는 마음뿐 입니다. 공부한다고 집안 대소사에 신경을 쓰지도 못하는 막내 아들에게 항상 괜찮다는 말만 반복하시던 부모님. 제가 꼭 원하는 것을 이루어서 그 동안 못해드린 것 다 해드릴 수 있었으면 좋겠습니다. 그리고, 제가 집안일에 소홀한 것을 대신 해주고 항상 힘이 되어준 형과 형수님께도 고마움을 전합니다. 이제 많이 커버린 소향이와 이제 곧 태어날 둘째 조카의 앞날에도 좋은 일만 있기를 간절히 바랍니다.

그리고, 하나 밖에 없는 외동딸을 저에게 보내시고 항상 걱정을 하시는 장인, 장모님께도 감사 드립니다. 공부한다는 핑계로 귀한 딸 고생시키는 못난 사위에게 항상 따뜻한 말씀과 넉넉한 웃음으로 기운을 주시는 장인어른과 장모님께 부끄럽지 않은 사위가 될 수 있도록 더욱 더 노력하는 모습 지켜봐 주셨으면 좋겠습니다. 또, 어려운 처남 매제 사이인데, 남들이 신기 할 정도로 마음을 터 놓고 지낼 수 있도록 해주시고 스트레스 받을 때마다 말벗이 되어주고 항상 열심히 해서 성공하라는 말을 하면서 다독여주신 상돈 형님과 밤늦게 불쑥 불쑥 찾아가도 반갑게 맞아주시며 웃음을 보여주신 아주머니께 고마움을 전합니다. 무럭무럭 자라나는 소현이의 앞날에도 기쁨만 가득하길 빕니다. 그리고 묵묵히 옆에서 지켜봐준 상윤이에게도 고마움을 전합니다.

마지막으로, 못난 남편 뒷바라지 하느라 고생만 하고 있는 나의 사랑하는 아내 혜민이에게는 너무나 미안한 마음뿐 입니다. 공부라는 기약 없는 길을 선택한 못난 남편에게 항상 기운 내라고 옆에서 응원해주고 힘든 내색 없이 모든 것을 꿋꿋이 참아 주었기 때문에 지난 2 년간의 석사과정을 무사히 마칠 수 있었던 것 같습니다. 아직 모든 것이 끝난 것은 아니지만, 조금만 더 고생해서 꼭 남보란 듯이 예쁘게 살 수 있도록 더욱 더 노력 할 것 입니다.

끝으로, 모든 분들께 감사 드리는 마음을 보답 할 수는 없지만, 이 논문으로나마 고마움 마음을 전하고 싶습니다. 모든 분들의 앞날에 기쁨만 가득하길 간절히 바랍니다.

2010 년 02 월

List of Papers

◈ Proceedings of Annual Conference

1. “The development of numerical model of nearshore current by using nonlinear combined refraction-diffraction model”, *Proceeding of the Korean Annual Conference on Civil Engineering*, pp. 4203 – 4206, 2008 (in Korean)
2. “The Nearshore Current Analysis in Gangjeong Waters Established An Artificial Reef”, *Proceeding of the Korean Association of Ocean Technology Societies Conference*, 2009, pp. 2424 - 2427
3. “Numerical Study on the Nearshore Current considering Wind Stress”, *Proceeding of the Korean Annual Conference on Civil Engineering*, pp. 2933 - 2936